**ANKARA YILDIRIM BEYAZIT UNIVERSITY**

**GRADUATE SCHOOL OF NATURAL AND APPLIED SCIENCES**


# ON-CHIP CELL WALL SEPARATION USING MAGNETIC NANOPARTICLES

**M.Sc. Thesis by**

**Yasin ÖZTÜRK**

**Department of Material Engineering**

**August, 2020**

**ANKARA**

# ON-CHIP CELL WALL SEPARATION USING MAGNETIC NANOPARTICLES

**A Thesis Submitted to**

**The Graduate School of Natural and Applied Sciences of**

**Ankara Yıldırım Beyazıt University**

**In Partial Fulfillment of the Requirements for the Degree of Master of Science in Material Engineering, Department of Material Engineering**

**by**

**Yasin ÖZTÜRK**

**August, 2020**

**ANKARA**

## THESIS EXAMINATION RESULT FORM

We have read the thesis entitled **"ON-CHIP CELL WALL SEPARATION USING MAGNETIC NANOPARTICLES"** completed by **YASİN ÖZTÜRK** under the supervision of **ASSIST. PROF. DR. FATMA DOĞAN GÜZEL** and we certify that in our opinion it is fully adequate, in scope and in quality, as a thesis for the degree of Master of Science.

Assist. Prof. Dr. Fatma DOĞAN GÜZEL

Supervisor

Assoc. Prof Dr. Hüseyin AVCI

Jury Member

Assist. Prof. Dr. Metehan ERDOĞAN

Jury Member

Prof. Dr. Ergün ERASLAN

Director

Graduate School of Natural and Applied Sciences

# ETHICAL DECLARATION

I hereby declare that, in this thesis which has been prepared in accordance with the Thesis Writing Manual of Graduate School of Natural and Applied Sciences,

- All data, information, and documents are obtained in the framework of academic and ethical rules,
- All information, documents, and assessments are presented in accordance with scientific ethics and morals,
- All the materials that have been utilized are fully cited and referenced,
- No change has been made on the utilized materials,
- All the works presented are original,

and in any contrary case of the above statements, I accept to renounce all my legal rights.

**Date:** **Signature: ……...**

**Name & Surname: Yasin Öztürk**

# ACKNOWLEDGEMENTS

I would like to express my sincere gratitude to my advisor Dr. Fatma Doğan GÜZEL for the continuous support, providing me with the unique opportunity to work in the research area of Lab-on-chip technology, for her mentorship and encouragement.

I would like to thank Dr Araz Norouz Dizaji, Dr. Hamed Ghorbanpoor, Dr. Aliakbar Ebrahimi, İremnur Akçakoca for their generous help for this research also for their friendship and companionship. I would like to also thank my family for their life-long love and support.

The research in this dissertation was supported by TUBITAK under the Grant No: 217S793.

**2020, 12 August** **Yasin ÖZTÜRK**

# ON-CHIP CELL WALL SEPARATION USING MAGNETIC NANOPARTICLES


## ABSTRACT

The separation of bio-particles has increased its importance in recent years. The conventional techniques such as centrifugation is still widely used. The microfluidic chips accompanying nanoparticle separation methods considerably increases the possibility of reducing the time of centrifugation. In this thesis, on-chip magnetophoretic bacterial cell wall separation is presented. In particular, passive micromixing and active separation of cell wall content from the cytoplasmic content of one of the gram-positive bacteria, *Staphylococcus aureus,* was investigated using magnetic nanoparticles on-chip to serve for more qualified nucleic acid content to examine. To do so, Vancomycin functionalized superparamagnetic iron oxides (Vanco-SPION) nanoparticles were used for the cell wall separation in the range of 10 nm to 300 nm. On-chip studies were carried out using PDMS-made microfluidics chips. Both magnetic nanoparticles and microfluidics devices have unique properties of its own, allowing highly selective analysis within short duration. We believe that the presented results in this thesis pave the way towards effective biosensor based analysis of bacteria and related studies such as antimicrobial resistance.



**Keywords:** Superparamagnetic nanoparticles, iron oxide, magnetophoresis, bio-separation, microfludics.

# MANYETİK NANOPARTİKÜLLER KULLANILARAK ÇİP-ÜSTÜ HÜCRE ÇEPERİ AYRIŞTIRILMASI


## ÖZ

Biyolojik malzemelerin birbirinden ayırımı son yıllarda önemini gittikçe artırmakla birlikte, santrifüj gibi geleneksel teknikler ayırım için halen yaygın olarak kullanılmaktadır. Nano boyuttaki parçacıkları ayırmaya olanak sağlayan mikroakışkan çipler, santrifüj süresini yüksek oranda azaltabilmektedir. Bu tezde, mikroakışkan çip kullanılarak manyetoforetik bakteri hücre duvarının ayrımı amaçlanmıştır. Özellikle çip içerisinde pasif mikromiksleme ile birlikte hücre duvarının, bir gram-pozitif bakterisi olan *Staphylococcus aureus*'tan aktif olarak ayrıştırılması, daha kaliteli nükleik asit içeriğinin incelenmesine hizmet etmesi beklenmektedir. Bunun için çip içerisinde manyetik nanoparçacıklar kullanılarak ayrıştırma amaçlanmıştır. Vankomisin ile fonksiyonalize hale getirilmiş süperparamanyetik demir oksit (Vanco-SPION) nanoparçacıkları, 10 nm ila 300 nm aralığında sentezlenerek çip içerisinde hücre duvarı ayrımı için kullanılarak çip çalışmaları, PDMS bazlı mikroakışkan çipler ile gerçekleştirilmiştir. Hem manyetik nanoparçacıklar hem de mikroakışkan sistemler, kendine özgü benzersiz özelliklere sahiptir ve bunların birlikte kullanımı kısa sürede özellikle seçici analizlere izin verir. Bu tezde elde edilen sonuçların, bakterilere yönelik antimikrobiyal direnç araştırmalarının ve bununla birlikte kullanılan biyosensör tabanlı uygulamaların önünü açtığına inanıyoruz.



**Anahtar Kelimeler:** Superparamanyetik nanopartikül, demir oksit, manyetoforez, biyo-ayrıştırma, mikroakışkanlar.

# CONTENTS

# NOMENCLATURE

## Roman Letter Symbols

| | |
|---|---|
| $H$ | Magnetic field strength |
| $M$ | Magnetization |
| $V_m$ | Scalar magnetic potential |
| $F_m$ | Magnetic Force |
| $F_d$ | Drag Force |
| $F_g$ | Gravitational Force |
| $F_b$ | Brownian force |
| $m_p$ | Mass of the particle |
| $B$ | Magnetic flux density |

## Greek Letter Symbols

| | |
|---|---|
| $\mu_0$ | Relative permeability of air |

## Acronyms

| | |
|---|---|
| *pDEP* | Positive dielectrophoresis |
| *nDEP* | Negative dielectrophoresis |
| *AC* | Alternating current |
| *DC* | Direct current |
| *SPION* | Superparamagnetic iron oxides |
| *NP* | Nanoparticle |
| *DI-$H_2O$* | Deionized water |
| *TMAOH* | Tetramethylammonium hydroxide |
| *THF* | Tetrahydrofuran |
| *UV* | Ultraviolet |
| *PDMS* | Polydimethylsiloxane |
| *PR* | Photoresist |
| *PG* | Propylen glycol |
| *EG* | Ethylene Glycol |
| *XRD* | X-ray Diffraction |

# LIST OF TABLES

# LIST OF FIGURES

# CHAPTER 1

## INTRODUCTION

In the second half of the 19th century, nanotechnology and related concepts began to become more evident. Especially with the invention of atomic microscopes, better visualization of the atomic and crystal structure of matter has made the production of nanoscale materials even easier [1]. The production of nanoscale materials occurs through two approaches. These are top-down and bottom-up approaches. Top-down approach, which engineers have used for years to produce machinery, also aims to miniaturize and use materials from micro or macro scale [2]. Lithography and the production of Microelectromechanical systems (MEMS) can be a good example for top-down approach. Bottom-up approach is the process of assembling atomic and molecular sequences with a certain pre-constructed design. Self-assemble and their forming a structure is a good example for this. Today, there are plenty of systems that apply both of these approaches on the same platform [3]. Thanks to the lab-on-chip technology, mobilization of nanoparticles in a miniaturized chips becomes possible.

Functionalized nanoparticles have been used for years in biomedical area. The ability to synthesize structures such as core-shell, core-shell-shell has also given us the ability to utilize the features of each. Applications such as drug targeting, drug screening, separation can be done with the help of interconnected elements [4]. It is possible to use properties such as electrical, surface and magnetic properties of nanoparticles and to design them according to the application with these methods. For example, in the $Fe_3O_4$-Au nanoparticle structure synthesized as a core-shell, it is possible to use more than one properties by using the magnetic properties of the core and the surface functionalization properties of Au in water [5].

Microfluidic technology is an emerging technology that is increasingly used today. By using the properties of flow phenomena at the micron level, studies such as multiple sensor applications, single cell and single molecule studies can be performed [6]. Photolithographic techniques are generally used for producing transparent microfluidic chips with feature sizes below 1mm. Lab-on-a-chip technology gives us

a great advantage of applications such as separation, focusing, filtering, trapping, detection etc [7]. The presence of these combined systems in a miniaturized chip paves the way for specific applications. Considering these, it is possible to separate biomaterials with new methods and functionalized materials using microfluidic technology [8].

The content of this chapter about the thesis study includes background overviews of magnetic materials and on-chip bioparticle separation systems.

## 1.1 Magnetic Materials

Magnetic materials are divided into 4 categories. These are diamagnetic, paramagnetic, ferromagnetic and anti-ferromagnetic materials. Magnetic properties consist of the motion and constant magnetic moment of electrons [9]. Generally, magnetic materials have a multimagnetic domain structure [10]. However, when they are reduced to nanosize, they can show paramagnetism as a result of a single domain. The domains and the orientation of the induced magnetic moments are shown in Figure 1.1 [11].

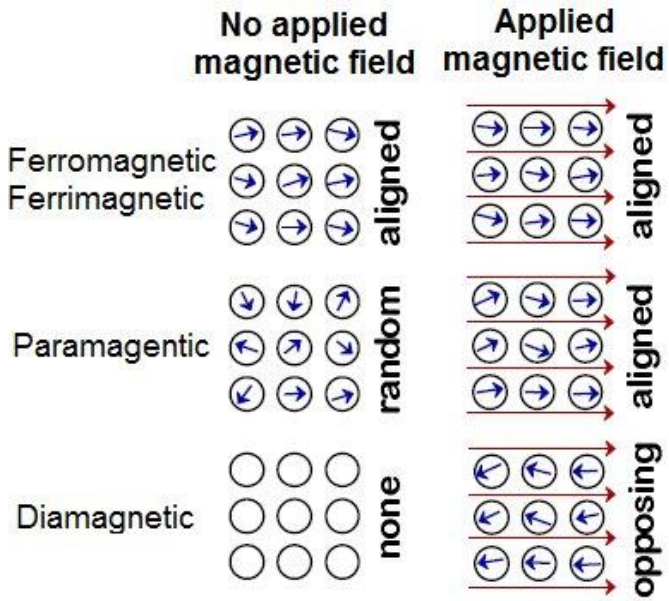


**Figure 1.1** Magnetism state of the materials and the magnetic orientations when external magnetic field applied or not.

Diamagnetism is a very weak state of magnetism. They have no net magnetic dipole moment. Relative permeability values of the diamagnetic materials have smaller than 1 and they have negative magnetic susceptibility. Superconducting materials have a superior form of diamagnetism in suitable temperature conditions [12].

Macroscopic magnetization of paramagnetic materials is zero in the absence of a magnetic field. In some solid materials, a constant dipole moment occurs as a result of electron spin. In the presence of magnetic field, the relative permeability value is slightly higher than 1 which they have proportional to the applied magnetic field [13].

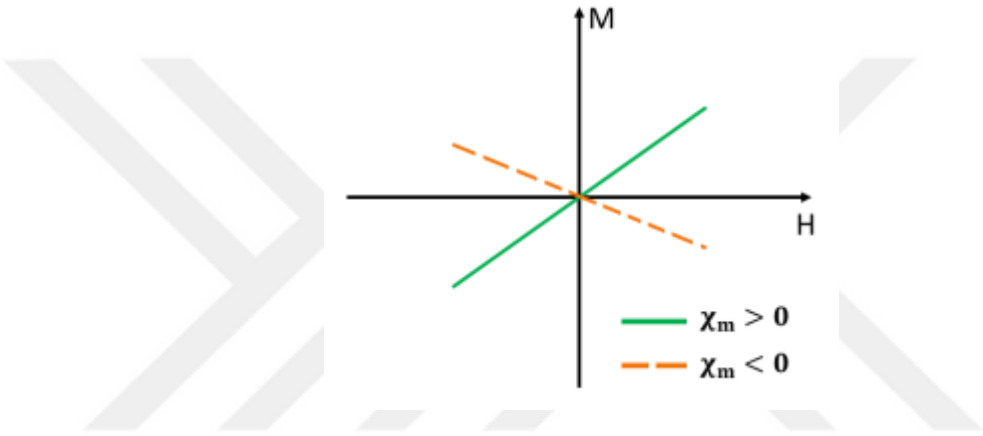


**Figure 1.2** Typical M-H curve of diamagnetic (orange) and paramagnetic (green) material.

Ferromagnetic materials are formed by arranging unpaired electron spins in parallel in a space called a domain. Ferromagnetic materials have a magnetization even no external magnetic field applied. This is called Remanent magnetization [14]. (Figure 1.3) When ferromagnetic materials encounter magnetic field, they show their magnetization for a while after absence of magnetic field. This magnetic recall state is indicated by the hysteresis loop.

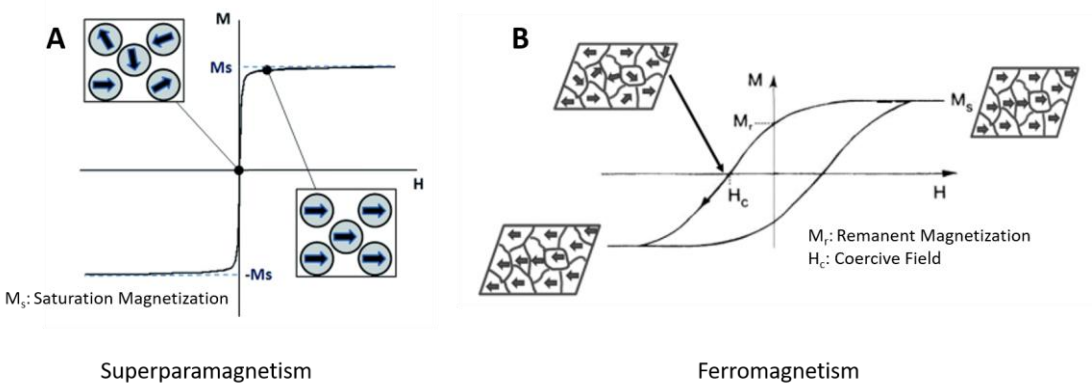


**Figure 1.3** M-H curve of superparamagnetic materials (A) and hysteresis loop of ferromagnetic materials (B).

Nano sized ferromagnetic materials can show superparamagnetism. With only the temperature variable, the magnetization orientation can change randomly [15]. The time taken during this change is called Neel relaxation time. The Neel relaxation time is smaller than the time required for magnetization measurement, making the material appear paramagnetic. This particular situation is called superparamagnetism. When external magnetic field is applied, the magnetic susceptibility of these materials is much higher than paramagnetic materials.

### 1.1.1 Magnetic Nanoparticles

Generally, magnetic nanoparticles are in the form of metal oxides and metal alloys. Magnetic compounds containing iron are widely used due to their magnetic saturation. Metal oxides NP includes iron oxides (($\gamma$-$Fe_2O_3$) and $Fe_3O_4$) and ferrites ($CoFe_2O_4$ and $Mn_{0.6}Zn_{0.4}Fe_2O_4$) [16]. Due to the nature of nanoparticle synthesis, the magnetic properties of these nanoparticles vary according to the synthesized dimensions. So their size and shape can be easily controlled by their synthesizing routes. Techniques such as co-precipitation, solvo-thermal, micelles and thermal decomposition are used as synthesis methods. These techniques change the magnetic properties and it is possible to produce narrow particle size dimensions [17-19].

Functionalized superparamagnetic iron oxides are widely used in biomedical applications such as biomolecule separation, drug targeting, drug screening and

Magnetic Resonance Imaging (MRI) applications [20]. Since it has high cytotoxicity in in vivo applications, its surface must be covered. For functionalization, methods such as gold, silane and polymer coatings are used for in vivo applications (Figure 1.4) [21].

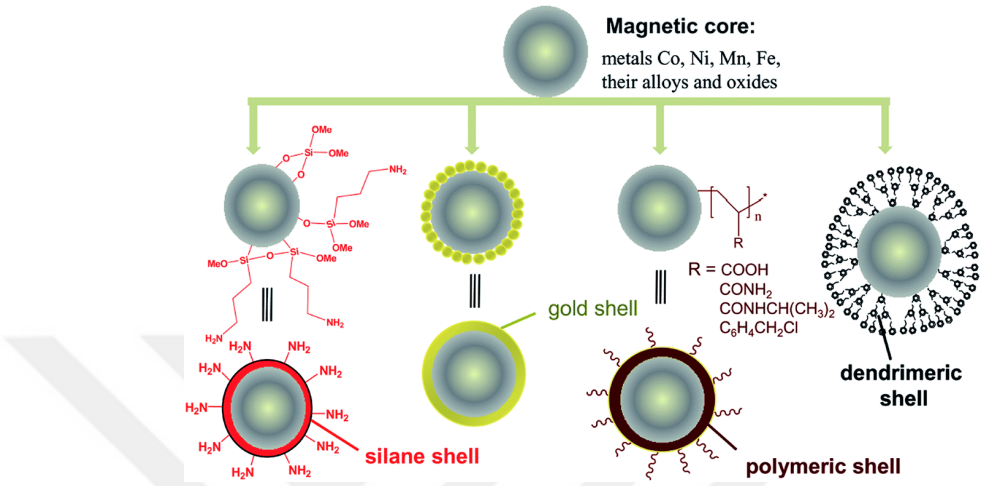


**Figure 1.4** Representative figure of core-shell structures of functionalized magnetic nanoparticles.

Unlike ferromagnetic materials, superparamagnetic iron oxides do not remain magnetic for a certain period of time when magnetic field is applied and cut. The use of magnetic resonance device is based on this situation [15]. In addition, finite elemental analysis has become easier thanks to this phenomenon [22].

## 1.2 On-Chip Bioparticle Separation

Microfluidic devices can be effectively used for the continuous separation of biomaterials and/or biomolecules [23]. This capability finds applications in many areas in industry such as pharmaceutical production centers and biotechnological fields [24]. There are several bio-particle separation techniques on-chip such as dielectrophoresis, electrophoresis and magnetophoresis [25]. These are active separation techniques which exhibit the external particle manipulation for the separation in microfluidics. The other separation approach is passive separation. It includes microfluidic designs with micropillars or designs that uses inertial forces such as channel design, materials density and hydrodynamic property of materials to separate the micro and nano(bio)materials [26].

Table 1.1 and Table 1.2 shows a summary of both reported techniques from the literature [27-32].

**Table 1.1** Active separation techniques.

| Method | Description | Scheme |
|---|---|---|
| Gravitational SPLITT | Separation field is possible but not adjustable because of the gravitation. | 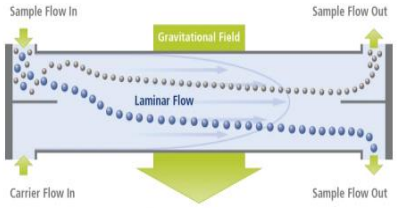  |
| | Separated: polystyrene beads, sea sediments. | |
| | Specified according to sedimentation behavior. | |
| Dielectrophoresis | Specified according to particle electric dipole. | 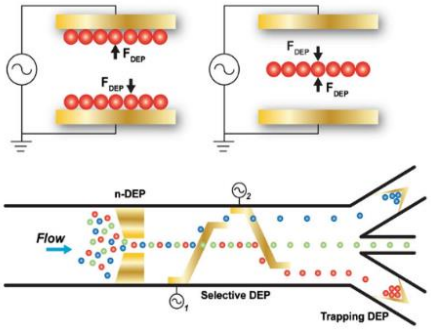  |
| | Uses non-uniform electric field. | |
| | Needs specific electrode design, can be 3D or layered electrode. | |
| | Distributed 2 categories: positive (pDEP) and negative (nDEP). | |
| | The magnitude and direction of the force depend on the gradient of electric fields and particle polarity. | |
| | The electric field can be AC or DC. | |
| Magnetophoresis | Biological materials can be separated by core-shell structures by the help of biological agents such as ligand attraction. | 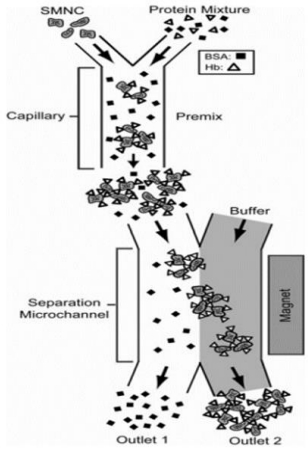  |
| | Superparamagnetic Nanoparticle (SPION) separation can be achieved with higher flow rates. | |

Dielectrophoresis is mostly used technique for the separation but it needs electrode design and expensive electrical and electronic equipment. However, magnetophoresis needs only permanent magnet or AC/DC (alternating current/direct current) controllable electromagnet. On the other hand, it is applicable only when the materials including paramagnetic or ferromagnetic materials that is influenced by the magnetic fields are used [33]. Within the scope of this thesis, we will focus on magnetophoresis in the next section.

**Table 1.2** Passive Separation Techniques

| Method | Description | Scheme |
|---|---|---|
| Density Based Separation | Density driven liposome separation can be achieved using this design. | 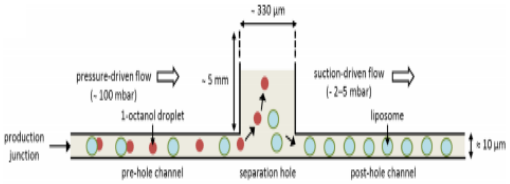  |
| Deterministic Lateral Displacement | Consists of pillar arrays structure which generates unique flow streamlines. | 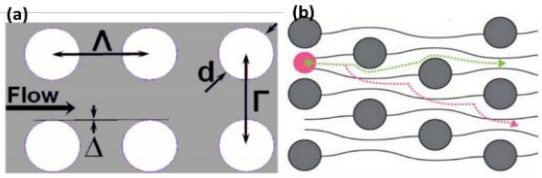  |
| | Circulating tumor cells, blood cells,mammalian cells, spores, parasites, and bacterias can be seperated by this design | |
| Inertial Microfluidics | Circulating tumor cells CTS separation can be achieved. | 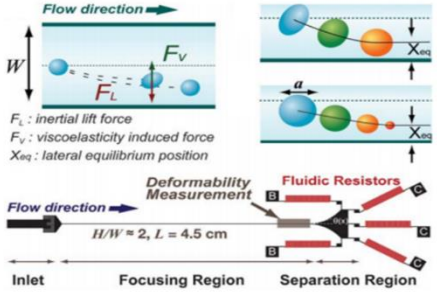  |
| | Forming inertial force on the particles in flow with using curved design. Large particles are expelled due to the moment of inertia, while small particles remain where they are compared to others. | |

## 1.3 Magnetophoresis

Magnetophoresis is an on-chip separation technique that uses magnetic fields to manipulate magnetic nanoparticles. Contactless and continuous separation of nanoparticles can be achievable when the magnetic particles are in microfluidic channel with flow. According to the effect of the particles on the magnetic field, magnetophoresis is characterized into two categories; negative and positive. Diamagnetic particle separation in the magnetic medium called negative, in case magnetic particle separation in diamagnetic medium is known as a positive magnetophoresis.

The key parameters effected on magnetic nanoparticles in fluid flow were given below. The magnetic force, is proportional to the external magnetic field. The relationship between magnetization and magnetic field and is represented by Equation 1.1.

$$\nabla\mu_0(\mathrm{H} + \mathrm{M}) = 0 \quad \textbf{(1.1)}$$

$$\mathrm{H} = -\nabla Vm \quad \textbf{(1.2)}$$

Where, ($\mu_0 = 4\pi \times 10^{-7}$, is the permeability of the air), H is magnetic field strength, M is magnetization of the particle, and $Vm$ is scalar magnetic potential. According to the mass conservation equation, it indicates that the liquid under steady state conditions and continuous flow conditions corresponds to the continuity equation and this is represented by;

$$\nabla(\rho f \mathrm{u} f) = 0 \quad \textbf{(1.3)}$$

Where $\rho f$ is density of the fluid and u$f$ is velocity of the fluid. Fluid behavior is presented by the Navier-Stokes equation;

$$pf(\mathrm{u}f.\nabla)\mathrm{u}f = -\nabla P + \nabla.(\eta.\nabla \mathrm{u}f) \quad \textbf{(1.4)}$$

Where $P$ is pressure and $\eta$ is the dynamic viscosity of the fluid. The migration of particles under an external magnetic field depends on the balance of forces acting on it. The main forces acting on the particle are the inertial force ($m_p d\mathrm{v}/dt$), the magnetic force ($F_m$), and the fluid drag force ($F_d$). For a shallow channel and an incompressible

fluid, gravitational force ($F_g$) and Brownian force ($F_b$) have little effect on particles. Therefore, not included in the calculations. For simplicity, total acting forces is shown by;

$$m_p \frac{dv}{dt} = F_m + F_d \quad \textbf{(1.5)}$$

Where $m_p$ is the mass of the particle, $v$ is the velocity of the particle, $F_m$ is the magnetic force, and $F_d$ is the viscous drag force. According to the Stokes law, the viscous drag force is determined as;

$$F_d = \frac{1}{\tau_p} mp(uf - v) \quad \textbf{(1.6)}$$

Where $\tau p$ (s) is the velocity response time of the particle, represented by;

$$\tau p = \frac{\rho p \; x \; dp^2}{18\mu} \quad \textbf{(1.7)}$$

Where $\rho p$ and $dp$ are the density and the diameter of the particle, respectively, $\mu$ is the fluid viscosity. Magnetophoretic force acting on the particle in a fluidic medium is then represented by;

$$F_m = (V(\chi - \chi_m)/\mu_0) \; x \; (\nabla . B)B \quad \textbf{(1.8)}$$

Where $\mu_0$ is magnetic permeability of the air, $V$ *is* particle volume, $\chi$ is magnetic susceptibility, $\chi_m$ is the susceptibility of the surrounding medium, and $\nabla$.B is field gradient of the magnetic flux density. As clearly seen, the magnetic force acting on the particles depends on the shape of the magnet and the distance to the microchannel - whether it is mobile or not- and the surrounding medium and the particle size. Magnetophoresis can be used in three different applications such as micromixing, separation and trapping [34-36]. Magnetic sources such as magnetic strip, permanent magnet, rotational permanent magnet, AC electromagnet were used in these applications inside the chip [30, 37].

"Karle et al. (2010)" performed the DNA extraction of *Escherichia coli* bacteria using rotational magnet and they achieved 147% on-chip separation yield according to the

off-chip experiments. Superparamagnetic beads were used to adhere to the surface of the extracted DNA [30].

In another continuous separation mechanism that modeled by Furlani (2006), AC electromagnet was created using an embedded soft electrode. White blood cells and red blood cells separation can be achievable with using magnetization of cells via hemoglobin oxygenation [36].

Magnetophoresis can also be used for mixing within the chip. “Wen et al. (2009)” aimed to enable ferrofluid-Rhodamine B functionalization by mixing Rhodamine B with ferrofluid with a 0.95 mixing index using AC electromagnet [37]. However, passive micromixing is possible with 3D soft microproduction method without using magnetophoresis and electrodes on the chip. “Tofteberg et al. (2009)” used 90 bends and T mixer together and at the same time, it was possible to reach 0.95 mixing index with the help of 3D angled barriers in PDMS based chip. This approach shows us that magnetophoresis and passive micromixing can be used simultaneously in the same microfluidic chip.

Capillary magnetophoresis method was developed by “Watarai et al. (2002)” to examine the magnetic susceptibility of red blood cells in manganese (II) solution. Red blood cells trapping mechanism has been developed by using an iron tip that transmits magnetism between two magnets inside the chip [38].

## 1.4 Motivation

The thesis includes functionalization of core-shell $Fe_3O_4$-Au nanoparticles with vancomycin antibiotic, which has the ability to specific binding to the surface of the *Staphylococcus aureus* cell wall. Ultimately, on-chip cell wall separation can be done using a permanent magnet with an ability to attract to the magnetic core of the functionalized nanoparticle.

Gram-positive and Gram-negative cell wall have a big difference in its peptidoglycan layer while considering the thickness of the layers surrounding the plasma membrane. Gram-negative peptidoglycan is only a few nanometers thick, representing one to a few layers (which surrounding with outer membrane layer), while Gram-positive

peptidoglycan is 30–100 nm thick and contains many layers. Therefore, in Gram-positive bacteria, cell wall to cell mass ratio can reach up to 60-40% [39]. This causes a great challenge when studying Gram-positive bacteria at the molecular level.

In order to enhance the efficiency of the analysis, one has to consider the cell wall separation from the cytoplasmic content of the bacteria. In this thesis, we therefore designed a methodology to separate the two content from each other, leading us to purified nucleic acid content to be used in further studies like antimicrobial resistance of the bacteria. We hypothesized that antimicrobial susceptibility sensors with enhanced efficiency can thus be developed the with nucleic acid purification.
Our methodology includes;

1. Synthesis of Superparamagnetic Iron-Oxide Nanoparticle (SPIONs)
2. Gold coating of the SPIONs
3. Chemical functionalization of SPIONs
4. Characterization of SPIONs
5. Off-chip cell wall separation using SPIONs
6. Microfluidic chip design and production
7. On-chip cell wall separation using SPIONs

The functionalized design of the SPIONs is as shown in the Figure 1.5.

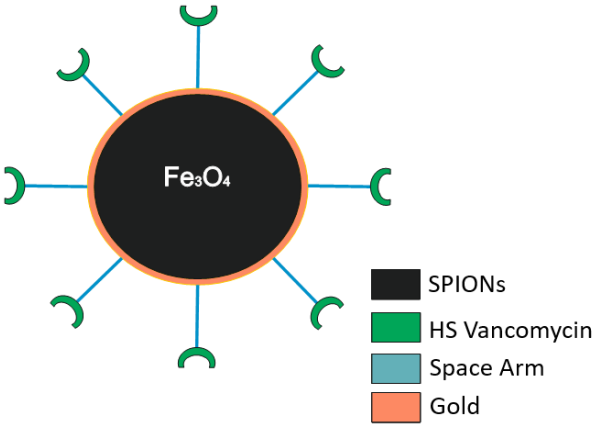


**Figure 1.5** The design of the vancomycin functionalized core-shell Au-$Fe_3O_4$ nanoparticle which it has ability to attach cell wall via vancomycin antibiotic.

# CHAPTER 2

## EXPERIMENTAL SECTION

In this section, experimental studies will be presented in 5 categories: Synthesis of the functionalized SPIONs, characterization of functionalized SPIONs, Production of Microfluidic Chips, Simulations, and off-chip and on-chip separation experimentation.

### 2.1 Synthesis of Functionalized SPIONs

#### 2.1.1 Synthesis of SPIONS

$Fe_3O_4$ nanoparticles (NPs) in three different sizes were synthesized (NPs-1, NPs-2, NPs-3). These were prepared by changing the experiment variables and medium. Solvo-thermal method was used for the synthesis of NPs. 30 mmol urea, 3 mmol $FeCl_3$ (Iron (III) chloride hexahydrate) and 1 mmol succinic acid were added to 30 ml of propylene glycol in a small beaker and mixed at 600 rpm for 15 minutes using magnetic stirrer (See Figure 2.1A). Then it was sonicated for 15 minutes and transferred into a custom-made Teflon chamber. Then, it was taken to the reactor made of stainless steel and its cover was tightened in order to ensure sealing (See Figure 2.1B). It was placed in an oven preheated to 200 ° C and left for 12 hours. Afterwards, it was left to cool down for half an hour after being removed from the oven. Then, NPs were separated from the medium by centrifuge method for 30 minutes at 10000 rpm and Ethanol was added after removal of the medium. Then it was taken into 2 ml eppendorf tubes and washed five times with DI-$H_2O$ with the help of magnetic separator. Finally, NPs were collected in a 20 ml glass tube. Then 15 µL of 0.1 M TMAOH (Tetramethylammonium hydroxide) was added and stored for further use at 4 °C (See Figure 2.1C and Figure 2.1D).

NPs-1 was synthesized using propylene glycol whereas NPs-2 and NPs-3 were produced in ethylene glycol, and were kept in the oven for 12 and 18 hours, respectively.

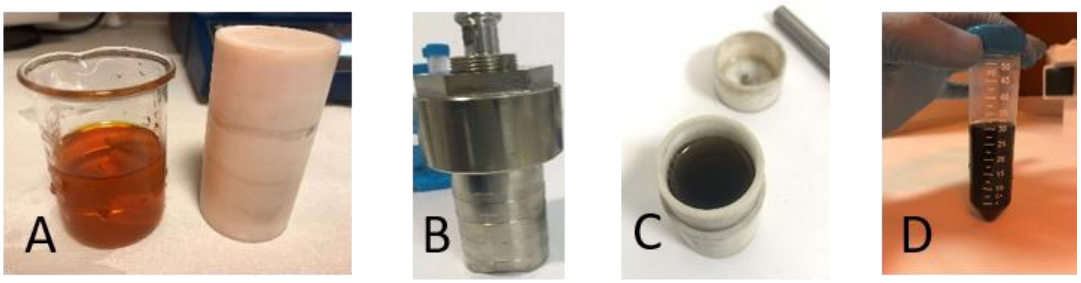


**Figure 2.1** SPION synthesis procedure. **A.** Solution ready for autoclave (left). Teflon Lining (right). **B.** Stainless steel reactor. **C.** After reaction. **D.** After added TMAOH and ready for use.

### 2.1.2 Synthesis of Gold Coated SPIONS

NPs were first washed with DI-$H_2O$ for five times; after which they were placed in 1 M nitric acid ($HNO_3$). The NPs containing $HNO_3$ solution were then boiled until their color changed from black to brown. $HNO_3$ was then removed with the help of magnetic separator. NPs in 0.1 M tri-sodium citrate were sonicated for 20 minutes. Immediately afterwards, it was thrown into the reactor made of Borosilicate glass, which was previously heated using silicone oil at 150 °C. It was stirred at 2000 rpm using a glass impeller. As soon as boiling started, 1 M $HAuCl_4$ (Gold (III) chloride trihydrate) was added every 5 seconds. When the color of the mixture turned into rose dry, it was waited for 15 minutes and separated from the silicone oil and continued to be mixed for 15 minutes. Process of the gold deposition is shown in Figure 2.2. Gold deposition was performed only for the synthesis of NPs-1 and NPs-3.

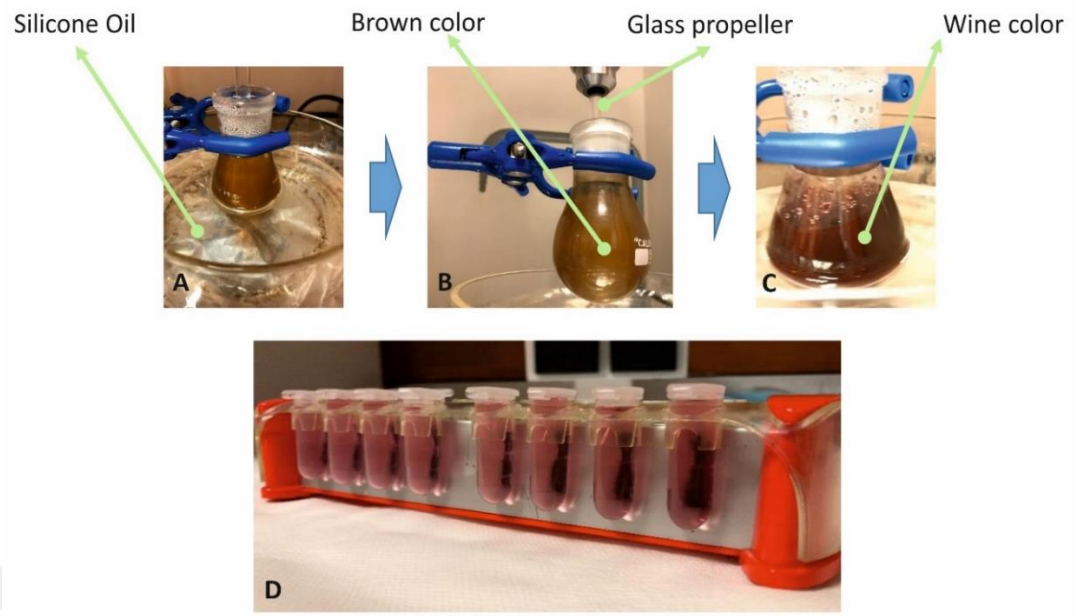


**Figure 2.2** Photography images of Au deposition of $Fe_3O_4$ nanoparticles. **A** and **B** represents nanoparticles before boiling by heater in tri-sodium citrate surrounding environment. **C.** After dropwise adding $HAuCl_4$. D: Washing step by using magnetic separator.

## 2.2 Synthesis of Bis-Vancomycin

The Bis-vancomycin synthesis was done according to "Norouz Dizaji et al. (2020)". 100mg Vancomycin was added to 1ml Dimethyl Sulfoxide (DMSO) in an eppendorf tube. Then, 6.8 mg Cystamine Dihydrochloride was added to 1 ml N, N-Dimethylformamide (DMF) and sonicated together for 15 minutes. First, the cystamine solution, then the vancomycin solution was added and mixed using the borosilicate glass reactor inside the ice bath. Mixing process was performed with magnetic stirrer at 300 rpm. Subsequently, 34 mg of N,N,N′,N′-Tetramethyl-O-(1H-benzotriazol-1-yl)uronium hexafluorophosphate (HBTU) and 60 µl of N,N-Diisopropylethylamine (DIEA) were added in 1 ml of DMF previously prepared in another eppendorf tube, and the resulting solution was added dropwise to the mixture after making sure it was dissolved by sonication. After the mixture was mixed in the ice bath for half an hour, it was removed from the ice bath and continued to stir overnight [40]. Process is shown in Figure 2.3.

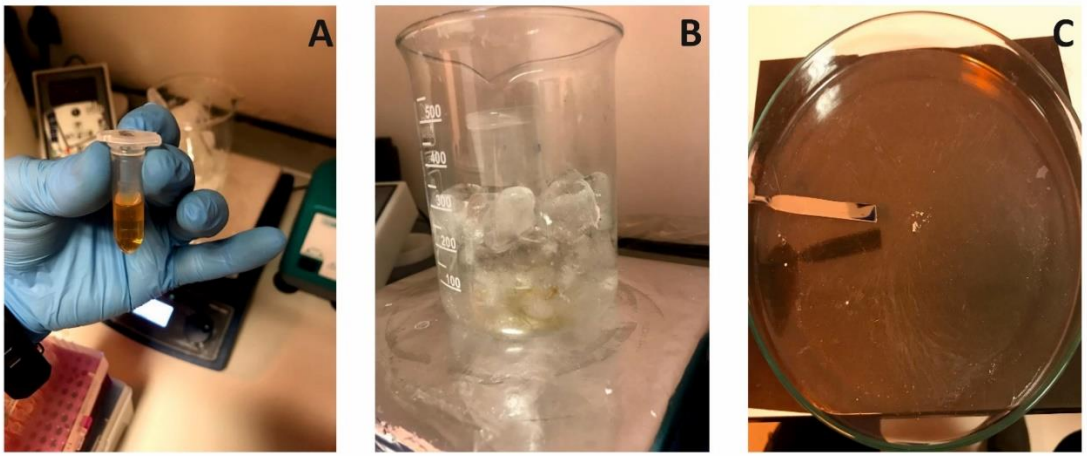


**Figure 2.3** Bis-Vancomycin synthesis photographs. **A.** Completely dissolved solution of HBTU and DIEA in DMF. **B.** Reactor in ice bath. **C.** Collecting via drying the Bis-Vancomycin after Prep-HPLC separation.

### 2.2.1 Bis-Vancomycin Purification

To remove unreacted molecules, Bis-Vancomycin molecules were collected in three vials using the C18 column with Preparative Liquid Chromatography (Prep-HPLC). Two different solutions were prepared for progress and separation throughout the column. The solutions were prepared with DI-H2O (%99.95) -THF (Tetrahydrofuran, %0.05) and methanol (%99.95) -THF (%0.05), respectively.

The Bis-Vancomycin solution collected in three vials was allowed to be vacuum-dried on a clean and flat glass at room temperature, and white residues adhering to the glass were collected eppendorf tube with the help of a spatula. After drying and harvesting, a total of 14 mg Bis-Vancomycin molecule was obtained. It was then lyophilized in an eppendorf tube at -80 °C for one day and stored at -20 °C for use in experiments.

## 2.3 Characterization of SPION and Bis-Vancomycin

The final solution including Bis-Vancomycin characterized Accurate-mass Q-TOF LC-MS (Agilent Technologies, Santa Clara, USA) in Institute of Materials Science and Nanotechnology (UNAM) at Bilkent University. After Prep-HPLC separation, Bis-Vancomycin molecules were further characterized in the Accurate-mass Q-TOF LC-MS device for confirmation.

Characterizations of molecular structure of obtained Bis-Vancomyxin were performed using X-Ray Diffractometry (XRD, Rigaku Miniflex, Japan) at Ankara Yıldırım Beyazıt University (AYBU). 200 µl of samples are dried with high vacuum on a flat glass. After drying, samples were placed on XRD device and 40kV / 15mA power, 0.02 angle stepper were adjusted, and total 90 degree measurements were taken.
Morphological characterizations were performed using Scanning Electron Microscope (SEM, Hitachi SU5000, Japan) and Transmission Electron Microscope at AYBU and Middle East Technical University(METU), respectively. For SEM sample preparation, 50 µl of SPION samples were dried on a flat glass. After drying, 1 nm gold sputtered onto the samples for electrical conductivity. For Au-$Fe_3O_4$ samples, they were not sputtered with gold for SEM sample preparation.

## 2.4 Production of Microfluidic Chips

### 2.4.1 Design of the Microfluidic Chip

Chips were designed using AutoCAD software and then transferred to the CORELDRAW software for the photomask space filling. Here, black and white areas for photomask were covered with "smart fill" tool, microchannels made transparent and other parts were covered in black (see Figure 2.4). The acetate photomasks were produced by Cozum Tanitim, Ankara. The size of the chips was 26 x 76 mm with the design area allowing offsetting the edges 2 mm inwards.

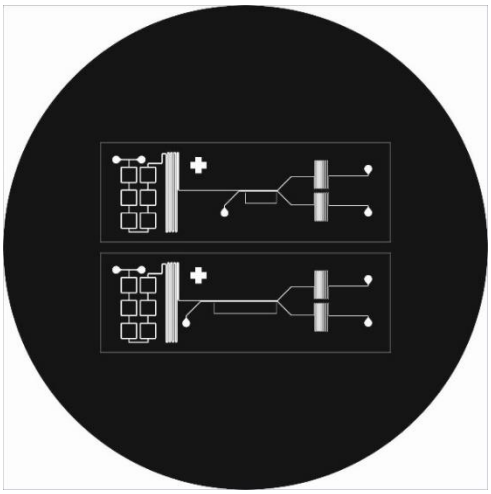

**Figure 2.4** Image of the 4-inch photomask**.**

### 2.4.2 Production of Si Template

Microfluidic chip templates were produced with SU-8 2050 (Microchem, USA) negative photoresist using traditional optical photolithography method. The production was carried out in the clean room. Photoresist was spin-coated on a 4-inch silicon wafer. The silicon wafer was uniformly coated with photoresist (PR) by rotating it at 500 rpm for 15 seconds and then for 30 seconds at 3000 rpm. After that, it was left for 65 minutes at 65 °C and 7 minutes at 95 °C, respectively, for soft bake. The mask was then placed on the wafer coated with the photoresist. To reduce the gap size in between the mask and the resists, sticky tape around the wafer and the mask was used.

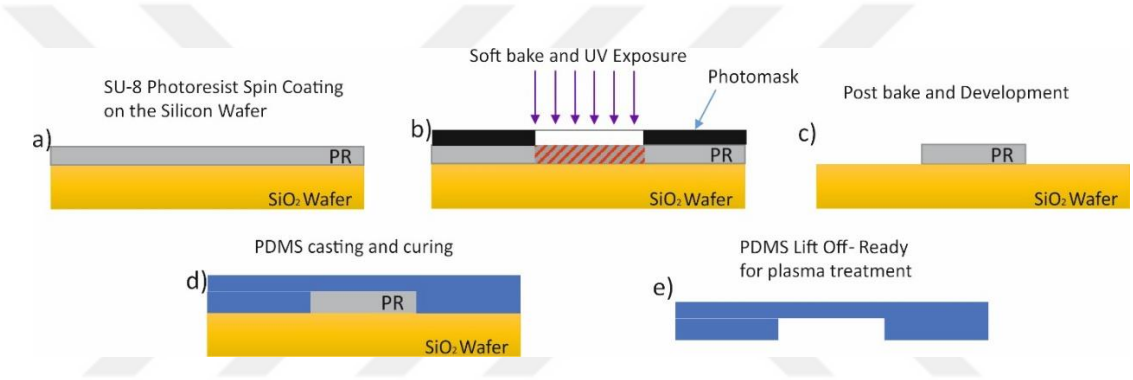


**Figure 2.5** General procedure of SU-8 photolithography for producing microchannels.

Wafer was exposed to the UV-light with a wavelength of 365 nm in a custom-made UV exposure setting. The setting contains a wafer console, timer and a 50W UV led that gives off at 365 nm wavelength, as seen in Figure 2.6A and Figure 2.6B. 180 second UV exposure was applied on the surface of the silicon wafer with photomask. After UV exposure was carefully taken over the photomask silicon wafer and kept on the hotplate for 1 minute at 65 °C and 6 minutes at 95 °C for post-bake treatment, respectively. Immediately after post bake process, wet etching process called develop was started.

50 ml of Propylene glycol methyl ether acetate (PGMEA) was poured into 6-inch beaker. Silicon template was put into PGMA and shaking for 5 minutes. Respectively Isopropanol (IPA) and deionized water was applied by squeezing for 10 seconds. It

was sufficient to apply 3-4 times. Then the front and back of the silicon wafer was dried with nitrogen gas.

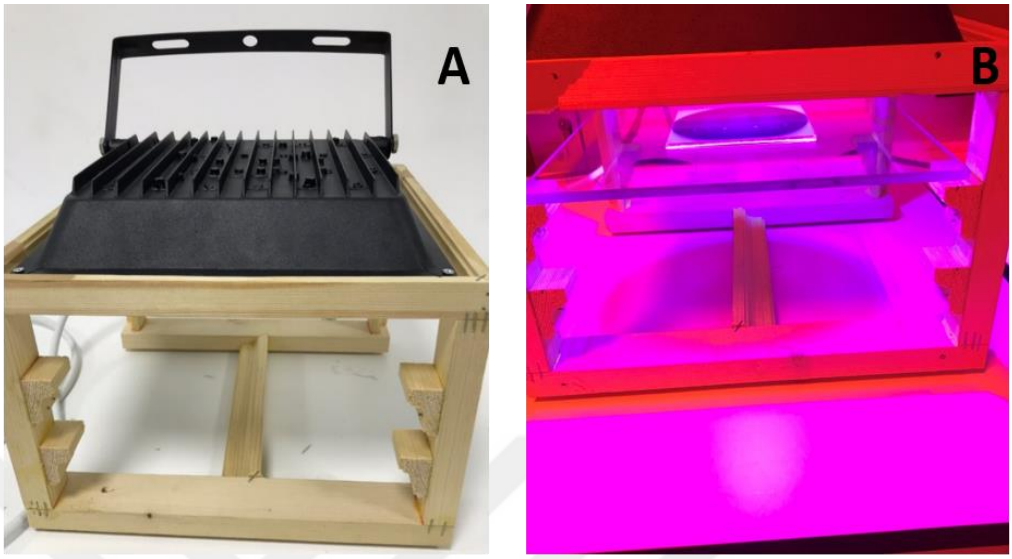


**Figure 2.6** UV exposure system. **A.** photography image of the device. **B.** Photography image of while exposing PR coated silicon wafer with photomask.

## 2.5 Production of PDMS-made Microfluidic Chips

Microfluidic chips were then produced using soft lithography process. Chips are made of epoxy-based polydimethylsiloxane (PDMS) and PDMS kit (Sylgard 184, Dow Corning USA) contains two components; base elastomer and the curing agent. Before the PDMS casting, a permanent magnet was placed right next to the separation channel, the locations of which were previously marked. Alignment was performed with another magnet at the bottom of the wafer with the help of a stereo microscope. PR patterned wafer was placed in glass dish after the magnet positioning, with the edges of the aluminum foil protruding. The reason for not being taken directly into the glass dish was to ensure that the lower magnet did not move. After alignment, PDMS base elastomer and the curing agent were mixed thoroughly at a 10:1 ratio and left in dessicator for 15 min to remove the air bubbles. Mixture was then poured onto the silicon template. PDMS thickness was adjusted in a way that the magnet's height was reached. Curing was carried out at 65 °C overnight. After the PDMS curing process, the magnet was separated and the cured PDMS layer at the top of the magnet was

peeled off gently. Magnet was removable and can be attached to the chip any time. The PDMS was chemically adhered to a clean glass slide and/or flat PDMS upon the plasma exposure.

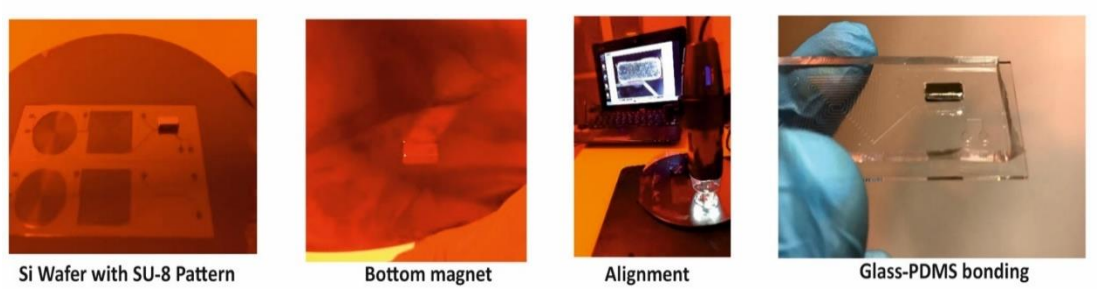


**Figure 2.7** Photography images of magnet alignment and glass-PDMS bonded chip.

In the hand-operated air plasma device, after the first two PDMS were placed, the borosilicate glass cover (See Figure 2.8B) was closed and the high vacuum pump was operated. Then, the microwave was operated and the plasma intensity was adjusted manually with the help of the variac device. Since 15-20 seconds of oxygen plasma light is suitable for PDMS-PDMS bonding, after 20 seconds, the microwave and vacuum are turned off and the air inside the desiccator is slowly filled. The microchannel PDMS, which was quickly taken on a flat surface, was placed on the flat PDMS and was pressed by hand for a while. To further enhance the adhesion, the glass/PDMS chip and/or PDMS/PDMS chips were left on a hot plate for one hour at 120 ° C.

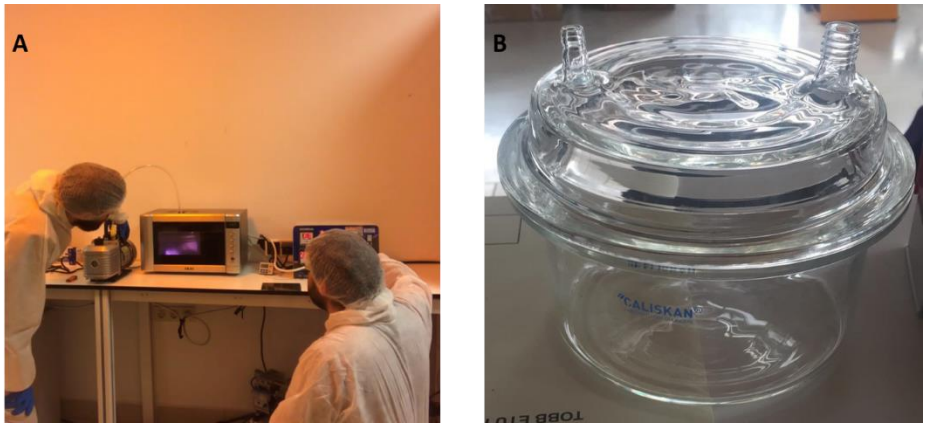


**Figure 2.8 A.** Air Plasma device. **B.** 8 mm thick borosilicate desiccator.

## 2.6 Simulations

Simulations were carried out using COMSOL Multiphysics 5.4 software. Particle variables were entered for permanent magnet, microchannel design and separation. The 2D design was saved in 2007 DXF version using AutoCAD 2018 and imported into the COMSOL program. Any possible design changes were made on AutoCAD. 6 modules were used in the COMSOL program. These modules and entered values were shown in Table 2.1, Table 2.2 and Table 2.3. Circular boundary was chosen for the simulations. There were two inlets. One of them was designed in a water medium with particles. The other inlet was used as buffer (water) inlet shown in Figure 2.9.

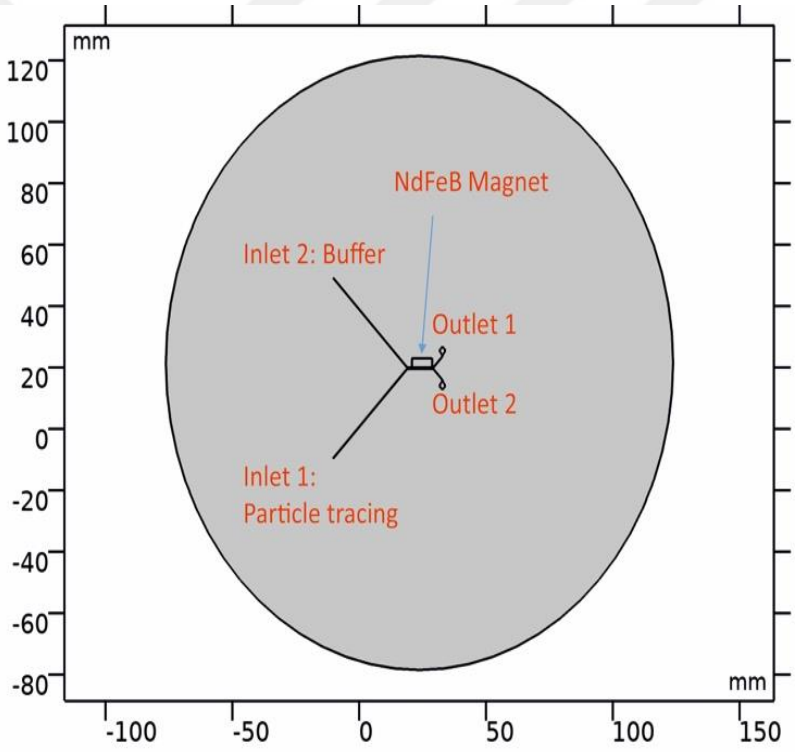


**Figure 2.9** Boundary and the design of the separation channel.

**Table 2.1** List of principle modules: geometry, materials and mfnc (magnetic fields, no currents).

| MODULES | | | Comments |
|---|---|---|---|
| Geometry | | | |
| Mathematical Object | Physical Object | Dimensions | |
| Circle (imported) | Boundry | r=10 cm | |
| Rectangle (imported) | Permanent Magnet | 8x3 mm2 | |
| 2D Closed Polylines | Microchannel | 60x50 mm2 | |
| Materials | | | |
| Material | Domains | | |
| Air (gas) | Domain 1 | | |
| H2O (water, liquid) | Domain 2 | | |
| Physical Module: Magnetic Fields, No Currents | | | |
| Details | | | |
| Magnetic Flux Conservation 1 | $\nabla \cdot \mathbf{B} = 0, \quad \mathbf{B} = \mu_0 \mu_r \mathbf{H}$ | Gauss law, Principal relation | For boundry conditions |
| | $\mathbf{H} = -\nabla V_m$ | Magnetic field and magnetic scalar potential | |
| Magnetic Insulation 1 | $\mathbf{n} \cdot \mathbf{B} = 0$ | | |
| Magnetic Flux Conservation 2 | $\nabla \cdot \mathbf{B} = 0, \quad \mathbf{B} = \mu_0 \mu_r \mathbf{H} + \mathbf{B}_r$ | Gauss law, Principal relation | For permanent magnet (NdFeB) |
| | | Relative permeability: 1.05 | |
| | | Remanent flux density= 1.32 | |
| | $\mathbf{H} = -\nabla V_m$ | Magnetic field and magnetic scalar potential | |

**Table 2.2** List of laminar flow module and their inputs.

| Physical Module: Laminar Flow | | | |
|---|---|---|---|
| Details | | | |
| Fluid Properties 1 | $\rho(\mathbf{u} \cdot \nabla)\mathbf{u} = \nabla \cdot [-p\mathbf{I} + \mathbf{K}] + \mathbf{F}$<br>$\rho \nabla \cdot (\mathbf{u}) = 0$<br>$\mathbf{K} = \mu\left(\nabla \mathbf{u} + (\nabla \mathbf{u})^T\right)$ | Navier-Stokes equations | Incrompressible fluid-flow |
| Wall 1 | $\mathbf{u} = \mathbf{0}$ | Velocity at the wall | Fluid Velocity at the wall was zero |
| Inlet 1 | $\mathbf{u} = -U_0 \mathbf{n}$ | Fluid Velocity = 2500[um/s] | Inlet velocities were typed |
| Inlet 2 | $\mathbf{u} = -U_0 \mathbf{n}$ | Fluid Velocity = 1000[um/s] | Inlet velocities were typed |
| Outlet 1 | $[-p\mathbf{I} + \mathbf{K}]\mathbf{n} = -\hat{p}_0 \mathbf{n}$<br>$\hat{p}_0 \le p_0$, | Outlet Pressure = 0 Pa | Outlet pressures set to be zero |
| Outlet 2 | $[-p\mathbf{I} + \mathbf{K}]\mathbf{n} = -\hat{p}_0 \mathbf{n}$<br>$\hat{p}_0 \le p_0$, | Outlet Pressure = 0 Pa | Outlet pressures set to be zero |

**Table 2.3** List of particle tracing - fluid flow module inputs.

| Physical Module: Particle Tracing for Fluid Flow | | | |
|---|---|---|---|
| Wall 1 | $\mathbf{v} = \mathbf{v}_c$ | vc is the particle velocity when striking the wall | Particle will stay when striking the wall |
| Particle Properties 1 | $\frac{d(m_p\mathbf{v})}{dt} = \mathbf{F}_t$ | Particle density = 5.24[g/cm^3] | |
| | | Particle diameter = 300 nm | |
| Magnetophoretic Force 1 | $\mathbf{F}_{mp} = 2\pi r_p^3 \mu_0 \mu_r K \nabla \mathbf{H}^2$ | Particle relative permeability = 1.09238 | |
| | $K = \frac{\mu_{r,p} - \mu_r}{\mu_{r,p} + 2\mu_r}$ | | |
| Inlet 1 | $\mathbf{q} = \mathbf{q}_0$ | | |
| | $\mathbf{v} = \mathbf{v}_0$ | | |
| Outlet 1 | $\mathbf{v} = \mathbf{v}_c$ | | |
| Outlet 2 | $\mathbf{v} = \mathbf{v}_c$ | | |
| Drag Force 1 | $\mathbf{F}_D = \frac{1}{\tau_p} m_p(\mathbf{u} - \mathbf{v})$ | | |
| | $\tau_p = \frac{\rho_p d_p^2}{18\mu}$ | | |
| MULTIPHYSICS | | | |
| Fluid-Particle Interaction 1 | $\mathbf{F}_v = -\sum_{j=1}^{N_t} n\mathbf{F}_D \delta(\mathbf{r} - \mathbf{q}_j)$ | | |

## 2.7 Off-chip and On-chip Separation Experiments

### 2.7.1 Preparation of Bacterial Culture

*S. aureus* were provided by Prof. Dr. Cihan Darcan from Bilecik University. A colony of bacteria was selected in LB Agar (Sigma-Aldrich, USA) medium and propagated in LB Broth (Sigma-Aldrich, USA) medium, stored at -80 °C in sterile eppendorf tubes. Broth medium was prepared for the bacterial medium. 25 grams of LB broth powder was mixed and dissolved in 1 L of distilled water at room temperature. Then, they were placed in Durham tubes in a large beaker and autoclaved with their caps at 135 °C for one hour. The caps of the homogenized liquid medium in the autoclave were closed and stored at 4 °C for later use. The nutrient medium at 4 °C was kept for

one hour in the incubator at 37 °C. Afterwards, the bacteria were then transferred to nutrient medium and kept in the incubator for 18 hours (See Figure 2.10). Turbidity method was used for bacterial count using a densitometer (Grant Instruments, USA). 0.5 McFarland ($1.5 \times 10^8$ cfu / ml) was prepared in a separate nutrient medium for all experiments.

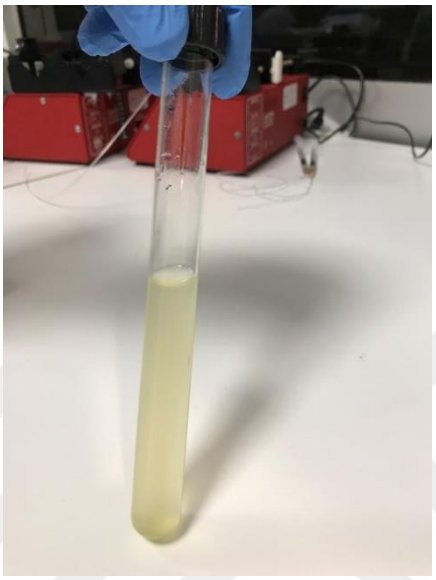

**Figure 2.10** A photography image of grown 5.0 McFarland bacterial cells in Durham tube after 18 hours of incubation.

### 2.7.2 Off-Chip Separation Experiments

Off-chip experiments were carried out using two different media (DI-$H_2O$ and ethanol) and the results were evaluated using NanoDrop device (Wilmington, Delaware USA).

In the first experiments, SPION-Au and S-Vancomycin incubation was performed in DI-$H_2O$. Then, lysed bacterial cells and SPION-Au-Vanco were incubated again in DI-$H_2O$ medium. The second experiments were performed with SPION-Au and S-Vancomycin incubation in ethanol. Then, non-lysed (nly) and lysed bacterial cells and SPION-Au-Vanco were incubated in separate experiments in the physiological saline solution.

To carry out the experiments in general, 1 mg of Bis-Vancomycin was dissolved in 2 ml DI-$H_2O$. 2 mg of TCEP (Tris(2-carboxyethyl) phosphine) was added to Bis-

Vancomycin solution and stirred for 1 hour at 600 rpm at room temperature. This allowed the thiol activation by breaking di-Sulphur bonds in Bis (Bisulfate, complex ligand with Sulphur central atom) state with the help of TCEP. Eventually, thiolated vancomycin (HS-Vancomycin) was obtained.

### 2.7.3 Off-chip Experiments in DI-H2O Medium

Gold-coated NPs were sonicated for half an hour in the containers, and different concentrations (2, 1, 0.5, 0.25, 0.125 ml) were taken into 2 ml glass tubes. It was washed twice with DI-$H_2O$ with the help of a magnetic separator and 900 µl DI-H2O was added to all of them and sonicated for 15 minutes. Then 100 µl of S-Vancomycin solution was added to all and sonicated. It was shaken once an hour for 12 hours. After 12 hours, S-Vancomycin molecules were washed once in the magnetic separator to separate them from the medium and 100 µl DI-$H_2O$ was added and sonicated again for half an hour.

Bacterial cells in broth medium were diluted in densitometer to 0.5 McFarland. then transferred to 2 ml eppendorf tubes. After centrifuging at 4000 rpm for 5 minutes, medium was removed and 1.6 ml DI-$H_2O$ was added to all of them. After they were all poured into a small beaker, 400 µl of non-lysed bacterial cells was taken and added to an Eppendorf tube containing 100 µl of DI-$H_2O$. Afterwards, bacterial cells were lysed by boiling in the heater for 5 minutes. Then, after adding 400 µl lysed content to all 100 µl SPION-Au-Vanco samples, they were mixed in shaking incubator at 200 rpm at 37 ° C.

After 3 hours and 12 hours, measurements were taken using the Nanodrop device separately. In the measurements, magnetic separator was used to examine the effect of SPION-Au-Vanco binding efficiency to the cell wall. To do this, 2 µl supernatant samples were measured one by one via UV spectrophotometry technique. The nucleic acid concentration and A260 / A280 ratios were examined for the nucleic acid purity.

### 2.7.4 Off-chip Experiments in Ethanol-Saline Medium

Unlike DI-$H_2O$ medium experiments, gold-coated NPs and S-Vancomycin were incubated for 12 hours in ethanol. In addition, physiological saline solution was used

instead of DI-$H_2O$ in bacterial cell experiments while other variables remained the same.

### 2.7.5 On-chip Separation Experiments

Experiments were carried out using two syringe pumps (New Era Pump Systems, NE-4002X, USA). While one contains a functionalized NP-Bacterial cell wall, the other was loaded with Buffer. The tips of 1 ml syringes were mounted on Polyethylene tubing (0.38mm ID, 1.09mm OD, Harvard Apparatus, USA) for the inlets. For the outlets, 200 µl pipette tips were mounted the chip. Chip is placed on optical microscope (inverted (Euromex oxion Inverso)) for looking at the separation channel. Experimental set-up can be seen in Figure 2.11.

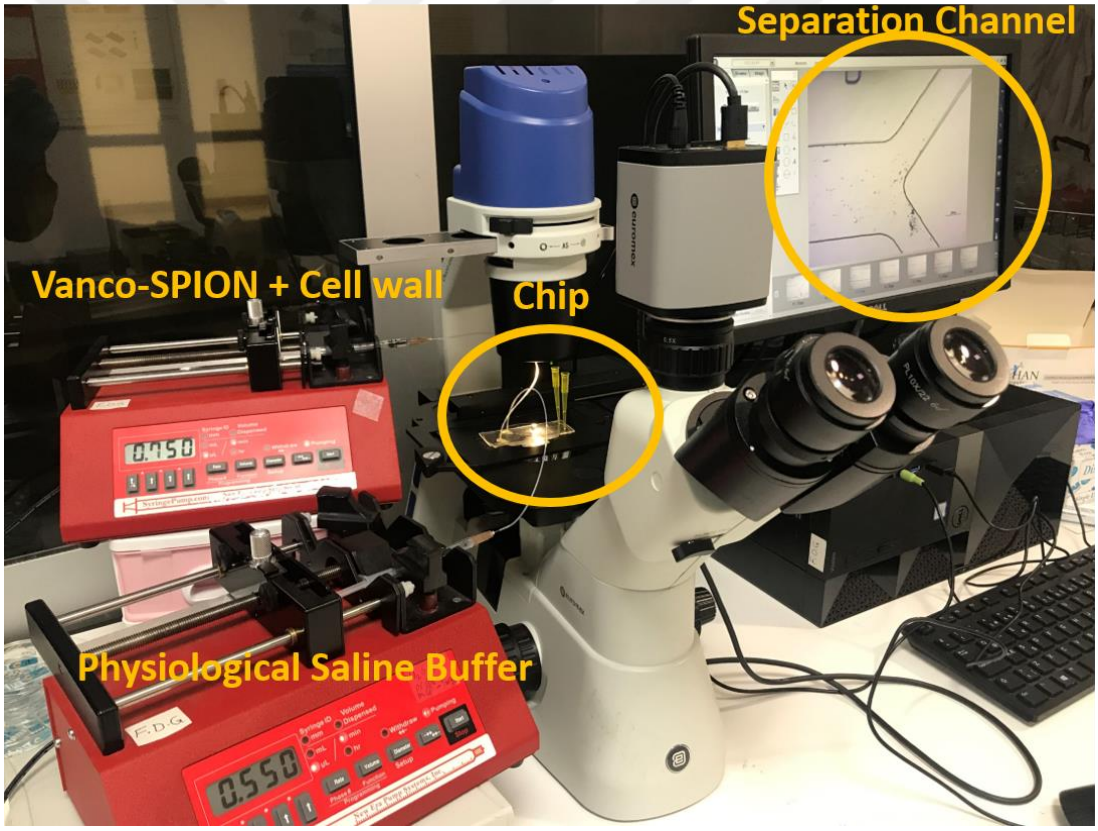


**Figure 2.11** Experimental set-up.

# CHAPTER 3

## RESULTS AND DISCUSSIONS

In this thesis, we aim to separate bacterial cell wall from the whole cell to investigate nucleic acid content without using detergents, elution buffers and centrifuging. Cell wall separation is aimed within the chip in a short time. The purpose of separating inside the chip using magnetic nanoparticles was to open the way of possibility to continuous and fast separation.

To do so, several experiments were carried out. In this section, we first present the results for the nanoparticle characterization. Chip production and simulation studies were then introduced. Finally, off-chip and on-chip separation results were discussed.

### 3.1 Nanoparticle Characterizations

Three types of synthesized $Fe_3O_4$ nanoparticles were named as NPs-1, NPs-2, and NPs-3 with an experimental yield of 4 mg / ml, 7 mg / ml, and 13.2 mg / ml. The other parameters and results can be seen at Table 3.1 below.

**Table 3.1** Table shows resulted parameters and synthesizing conditions of NPs-1, NPs-2 and NPs-3.

| | Au Deposition | Mean Hydrodynamic Diameter | Synthesized solvent | Structure | Concentration |
|---|---|---|---|---|---|
| NPs-1 | Yes | 30 nm | Propylene Glycol | Crystal-like | 4 mg / ml |
| NPs-2 | No | 50 nm | Ethylene Glycol | Flower-like clusters | 7 mg / ml |
| NPs-3 | Yes | 300 nm | Ethylene Glycol | Flower-like clusters | 13.2 mg / ml |

When the Ethylene glycol medium (EG, NPs-3) was used in the SPION synthesis stage, the nanoparticle size increased up to 310 nm. During synthesis with the

propylene glycol (PG, NPs-1) solvent, nanoparticles initially had faster nucleation than EG (Ethylene Glycol) and aggregation among the particles was faster. In EG solvent, this process was slower and the particles tended to rotate after nucleation, making them more suitable for self-assemble. Therefore, their size was larger and have a flower-like structure. Ostwald ripening process takes place in both solvents where misaligned particles dissolve in the solvent and growth occurs thermodynamically in the cluster. Thus, the growth process continues to a point [41]. The reaction of SPION synthesis using solvothermal method is called polyol reactions according to the solvents used. These reactions are shown below. Hydroxyl groups come from urea. Succinic acid acts as a catalyst and iron source comes from $FeCl_3$ [42].

$$RCHOHCH_2OH \rightarrow RCH_2CHO + H_2O \quad \textbf{(3.1)}$$

$$CO(NH_2)_2 + H_2O \rightarrow NH_4^+ + OH + HNCO \quad \textbf{(3.2)}$$

$$Fe^{3+} + 3OH \rightarrow Fe(OH)_3 \quad \textbf{(3.3)}$$

$$2RCH_2CHO + 2Fe(OH)_3 \rightarrow RCH_2COCOCH_2R + 2Fe(OH)_2 + 2H_2O \quad \textbf{(3.4)}$$

$$Fe(OH)_2 + 2Fe(OH)_3 \rightarrow Fe_3O_4 + 4H_2O \quad \textbf{(3.5)}$$

NPs were first characterized using XRD instrumentation. Powder XRD patterns of NPs-1 and gold coated NPs-1 were shown in Figure 3.1. Looking at XRD analysis, it can be said that most of the NPs-1 surface was covered with Au.

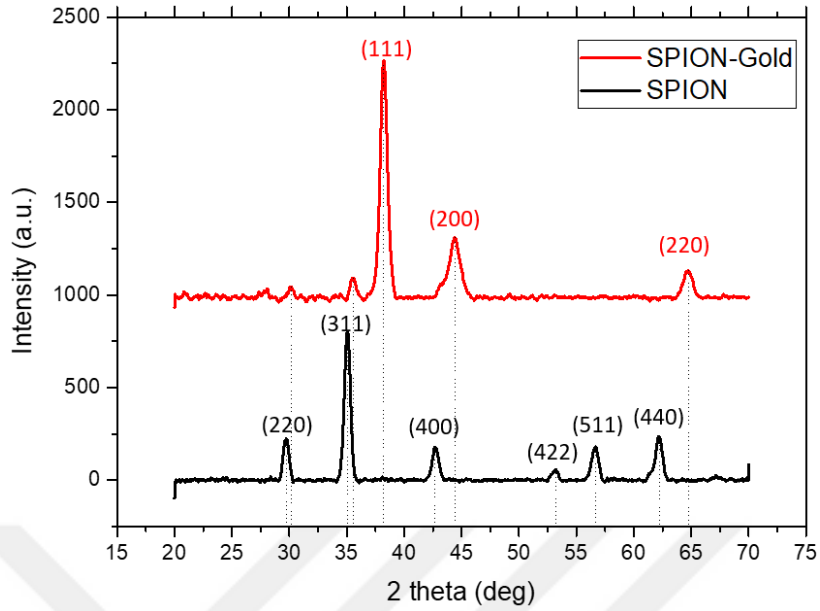


**Figure 3.1** Powder XRD patterns of NPs-1 and gold coated NPs-1. Characteristic peaks can be seen core-shell $Fe_3O_4$-Au nanoparticles. Black colored miller indices belong to $Fe_3O_4$, red ones Au.

Figure 3.2 shows the XRD results for gold coated NPs-3. It seems that $Fe_3O_4$ peaks also exist intensively. This may be due to the NPs-3 flower-like structure, the penetration depth of the XRD measurement or the fact that it was not fully oxidized with $HNO_3$ due to this structure before coating with gold. This may require additional studies. However, it is known that the gold deposition reduces saturation magnetization a lot as the thickness increases [43]. Considering that gold is not fully coated, both for immobilizing vancomycin and for magnetic efficiency, it was thought that this may work in on-chip experiments.

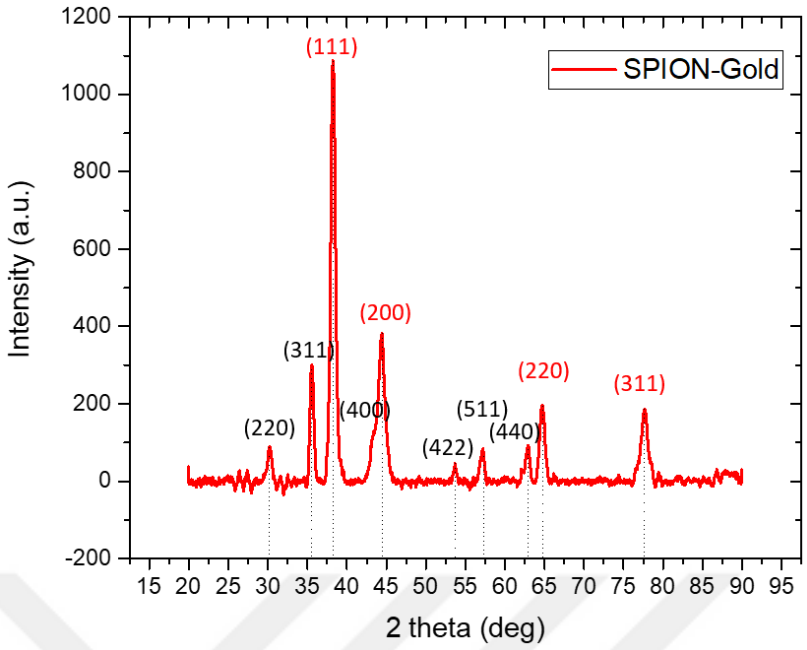


**Figure 3.2** Powder XRD patterns of NPs-3. Characteristic peaks can be seen core-shell $Fe_3O_4$-Au nanoparticles. Black and red colored miller indices belong to $Fe_3O_4$ and Au, respectively. Both of them can be seen at one gold deposited sample.

SEM images of the NPs, as seen in Figure 3.3 shows particle size distributions differ according to different solvents and reaction time used. Propylene Glycol with 12-hour reaction time gave us narrow PSD with crystal-like structure (Figure 3.3A). Ethylene Glycol with 18-hour reaction time gave us broader PSD with flower-like structure (Figure 3.3C)

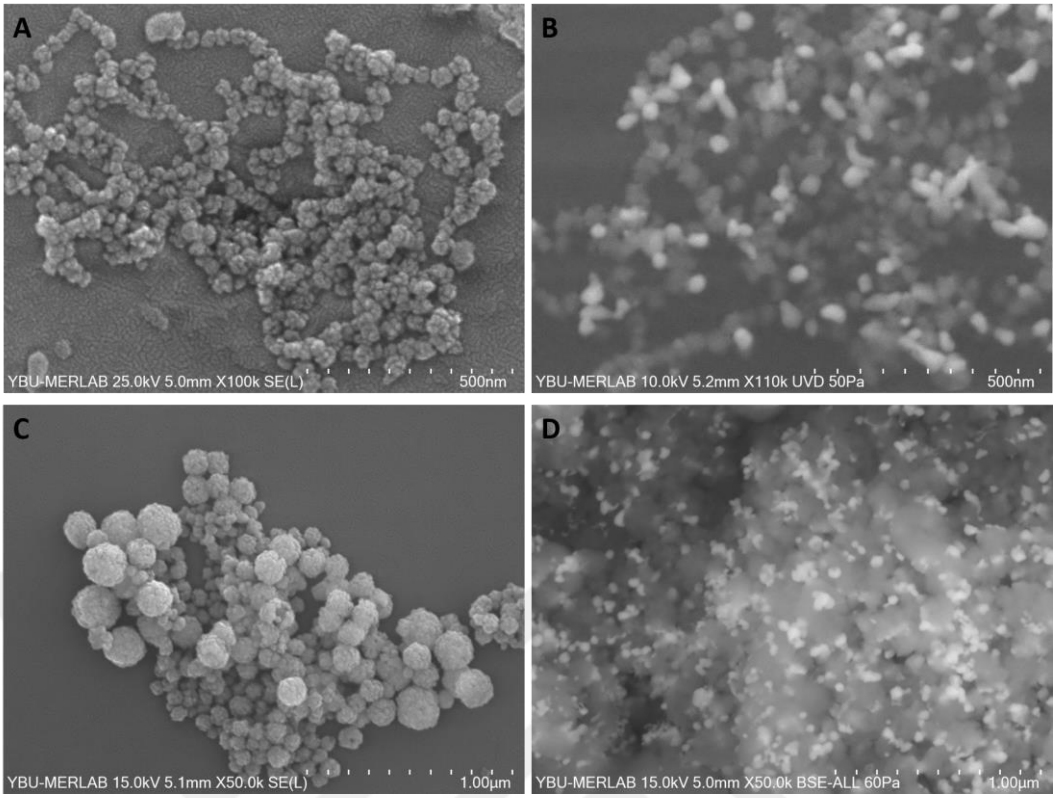


**Figure 3.3** SEM micrographs of synthesized $Fe_3O_4$ NP's and gold deposited $Fe_3O_4$ NP's. **B** and **D** were not sputtered with Au for SEM sample preparation. **A.** NPs-1 has narrow PSD around 30 nm. **B.** Gold deposited $Fe_3O_4$ (NPs-1). **C.** NPs-3 has flower-like structure and wide PSD and bigger sizes up to 310 nm. **D.** Gold deposited $Fe_3O_4$ (NPs-3).

In conclusion, NPs-1 and NPs-3 were synthesized separately in different sizes and particle size distributions. Evaluated according to the off chip results and the experiments continued by selecting the most effective concentration for on-chip.

## 3.2 Simulations

Magnetic materials react to the applied magnetic field. The relative permeability value is the measurable response of this magnetic field of the internal structure of the material. In ferromagnetic materials, this value is much more than 1. In superparamagnetic materials, it is slightly larger than 1 [44]. The relative permeability value is found by dividing the permeability value by the vacuum permeability ($4\pi 10^{-7}$ H x $m^{-1}$) (Equation 3.6) Permeability value can be found from magnetization curve by dividing flux density (B) by field strength (H) (Equation 3.7);

$$\mu_r = \mu / \mu_0 \quad \textbf{(3.6)}$$

$$\mu_r = (B / H) / \mu_0 \quad \textbf{(3.7)}$$

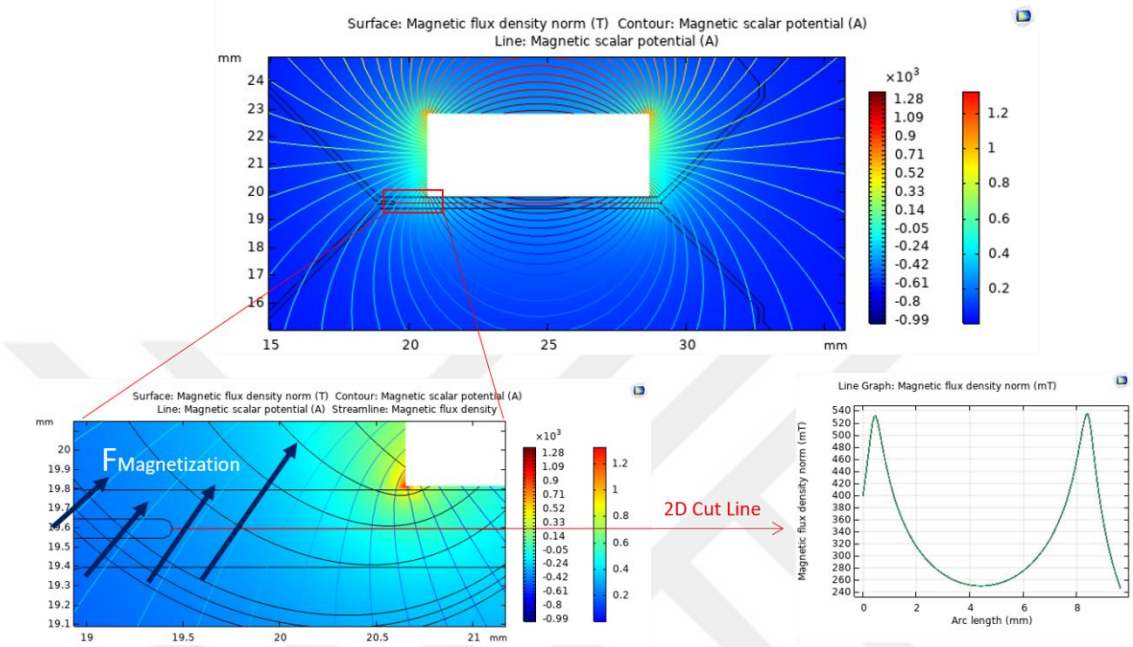


**Figure 3.4** 2D results of Magnetic flux density and magnetic scalar potentials of 8 x 3 mm NdFeB permanent magnet and cut line graph of magnetic flux density acting of microchannels.

It is very important to know the relative permeability value of the particles to be used for simulation, and this requires a B-H curve (Equation 3.7). VSM (Vibrating-sample magnetometer) device is suitable for obtaining the B-H curve. However, due to minor differences in material preparation and the effects of nanoparticles on each other, the relative permeability value may not be found precisely [45]. Therefore, this value was applied for nanoparticles in simulation by looking at the literature [46-48].

An 8 x 3 mm rectangular shaped NdFeB magnet was investigated to determine the location of the magnetic channel inside the chip, along with its distance to the channel, and how much the magnetic effect is. In the Particle Tracing module, only the size and values of the single particle were entered and particle-to-particle interaction was not calculated. We know that functionalized nanoparticles have a colloidal stability that

overcomes the electrosteric stabilization that comes with vancomycin [49]. Therefore, they tend to attract each other.

Simulation experiments were initially performed with a single channel and a single magnet. Thus, both laminar flow and magnetic module were tested together in simulation. After that, Particle Tracing Module was added and particle values were entered into the simulation. Particles emerging from a single inlet tended to move in the direction of the magnet 2mm away in the first second. To study the nature of the movement, the inlet was moved to a remote location within the boundary. So the particles coming out of the inlet encountered a little bit of magnetic force first hand. Particles approached the magnet and hit the microchannel wall early. Then, the separation channel design was added and a flow experiment was performed with two inlets and two outlets. With the buffer flow, the direction determination of the particles, which are under the effect of a new flow force, became easier. After that, the position of the magnet across the separation channel was adjusted according to the magnetic field acting on the particles coming from inlet1 (Figure 3.4). According to simulation results, the distance between the magnet and the separation channel has been reduced to 200 µm, considering chip production and magnet positioning possibilities. In addition, according to the position of the magnetic field lines, the separation channel was extended and the magnet was pulled 2 mm to the right.

As seen in the Figure 3.4, a line graph was drawn from the middle of the microchannel. The maximum magnetic flux density that will affect the nanoparticles was 525 mT. With this value, separation was achieved after revisions in the simulation. (Figure 3.5) Most effective simulation design was produced afterwards.

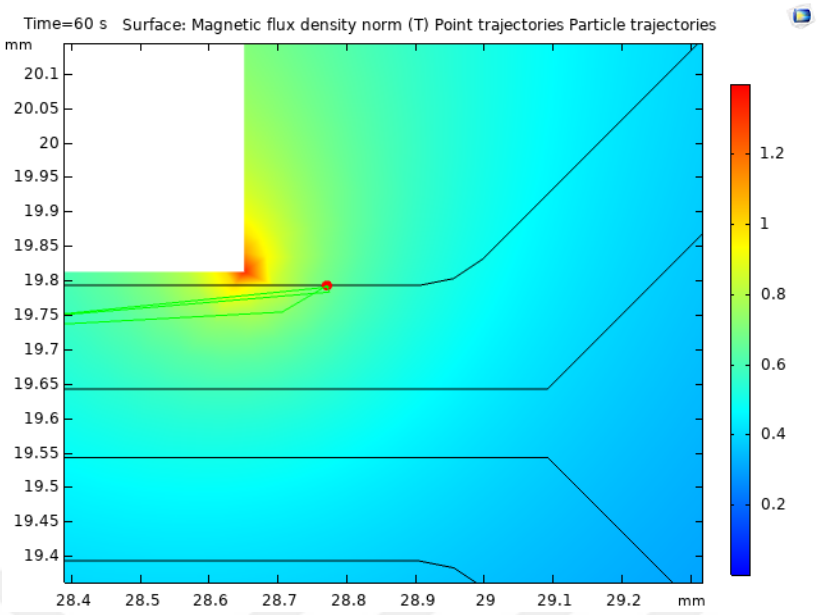


**Figure 3.5** Separated particle (300 nm in diameter) adhere to microchannel wall near the NdFeB magnet.

As results, we found that 525 mT was sufficient for separation of NP's in laminar flow. Also magnet location and channel dimensions were adjusted for the effectivity. For later simulations, the intermediate channel was used for better results. However, after on-chip experiments with intermediate channel, slight increase or decrease of the outlet pressures because of the fittings and tubes easily changed direction of the separation. To overcome this problem, the microchannels were extended from separation channel to the outlets. These channels were named pressure balancer as seen in Figure 3.11.

## 3.3 Optimization of the Chip Production

Several parameters in UV exposure system and photoresist protocol was varied to optimize the results and obtain the desired chip structures. In order to do so, the parameters as given in Table 3.2, were investigated and one of the experiment found to be optimal.

The pattern dimensions in the template were studied using Dektak profiler. Results are shown in Figure 3.6. It is clearly seen that the patterns of 42 microns were obtained successfully using the No 4 experiment. The feature type that we wanted to

appear is a rectangular type. The vertical plane is extended in order to see the wall slope more clearly in the profilometry results.

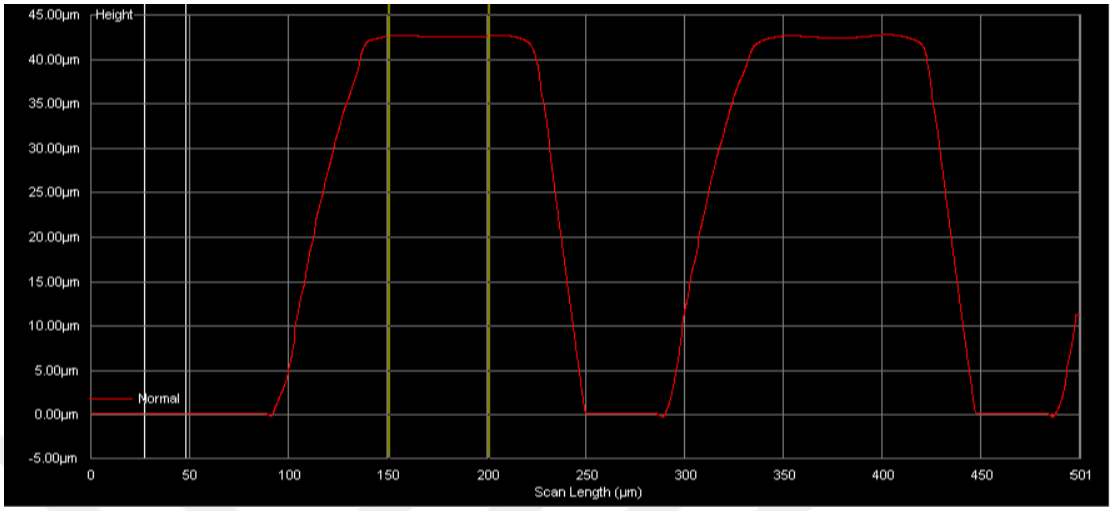


**Figure 3.6** Profilometry results. Feature height was about 42 µm.

In conclusion, 4th experiments were found optimal by analyzing wall slope. The slope increased when we increased the develop time in the same UV exposure time (180 sec). When we kept the develop time constant (3 min) and increased the exposure, it was observed that the slope increased in the same way. Accordingly, in the 4th experiment, the slope of the wall was higher than the others and gave the best result.

**Table 3.2** UV exposer optimization experiments for microfluidic chip production. Resulted thickness values was measured from 3 different parts of the same wafer and averaged.

| Experiment | 1. spin | 2. spin | Soft Bake | UV Exp. Time | Post Bake | Development | Resulted Thickness |
|---|---|---|---|---|---|---|---|
| 1 | 15sec/500 rpm | 30 sec / 3000 rpm | 3-7 min | 180 sec | 1-6 min | 3 min | 55±3 um |
| 2 | 15sec/500 rpm | 30 sec / 3000 rpm | 3-7 min | 180 sec | 1-6 min | 3.25 min | 60±2 um |
| 3 | 15sec/500 rpm | 30 sec / 3000 rpm | 3-7 min | 180 sec | 1-6 min | 4 min | 58±3 um |
| 4 | 15sec/500 rpm | 30 sec / 3000 rpm | 3-7 min | 180 sec | 1-6 min | 5 min | 42±1 um |
| 5 | 15sec/500 rpm | 30 sec / 3000 rpm | 3-7 min | 170 sec | 1-6 min | 3 min | 47±3 um |
| 6 | 15sec/500 rpm | 30 sec / 3000 rpm | 3-7 min | 190 sec | 1-6 min | 3 min | 47±3 um |

## 3.4 Separation Analysis

### 3.4.1 Off-chip Separation Analysis

Nucleic acid purity can be examined by spectrophotometric analysis method. Protein contaminant ratio can be found especially by comparing UV absorbance rates. The A260 / A280 ratio, i.e. the ratio of 260 nm absorption at 280 nm, gives us information about purity. This ratio is expected to be between 1.8 and 2.0 [50]. The measurements taken on the NanoDrop spectrophotometer device are given on the threshold of 1mm absorbance. During the DI-$H_2O$ experiments, cell lysis was performed by heating method and nucleic acid concentration were generally 4-9 ng / µl. According to the standard deviations of the spectrophotometer, when working with these nucleic acid values, the deviation increases up to about 10 percent. Minimum working range 10 ng / µl is recommended for DNA concentration. Therefore, it was necessary to make efficient cell lysis later.

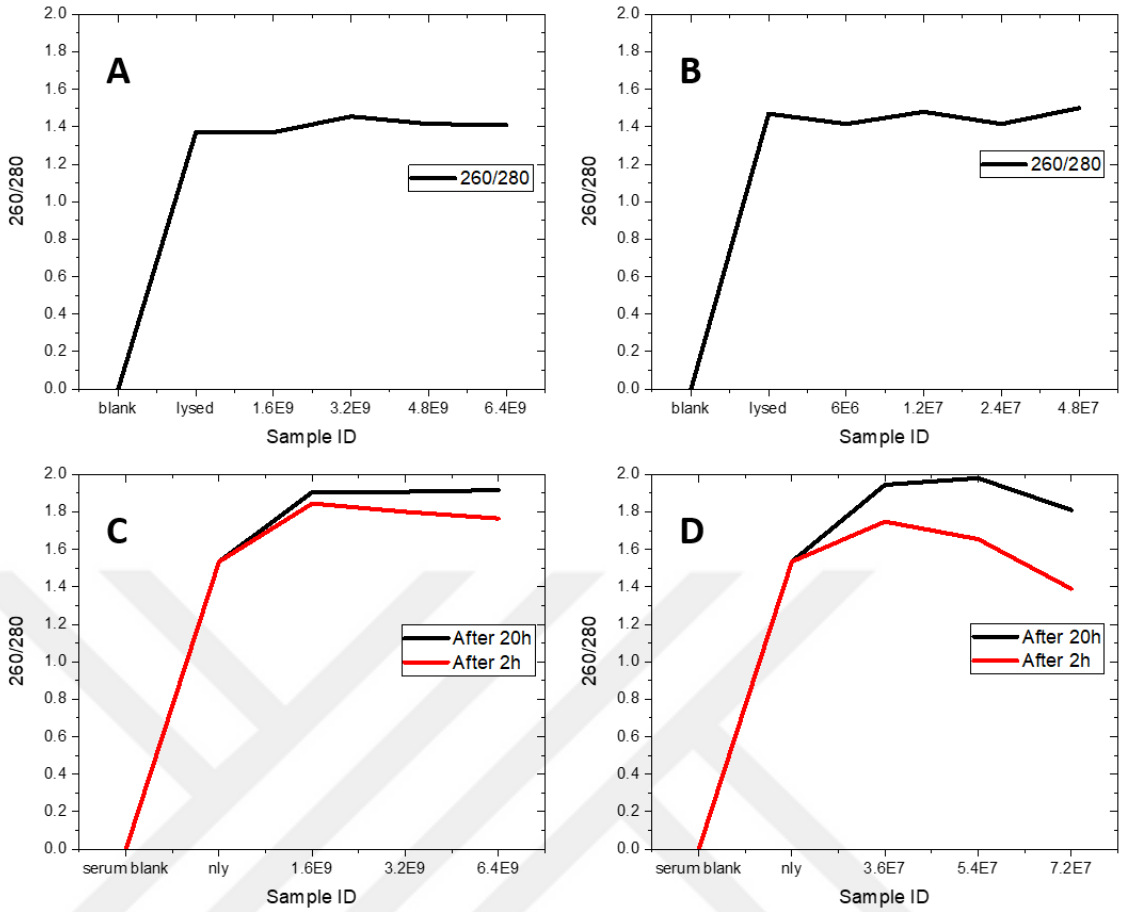


**Figure 3.7** A260 / A280 spectrophotometric results. Sample ID's are the average number of NP's calculated. All experiments were performed with an average amount of 7.5 x $10^7$ *staphylococcus aerus* cells. **A** and **B** corresponds to off-chip DIW medium experiments for NPs-1 and NPs-3, respectively. **C** and **D** corresponds to off-chip ethanol-saline experiments for NPs-1 and NPs-3, respectively.

The reason why detergents are not preferred for cell lysis is because of the possibility of dissolving the cell wall and breaking it down. Probe sonication was preferred by looking at physical disruption methods. In this way, physical lysis was made efficiently. When we look at the literature, mostly DI-$H_2O$ and ethanol environments have been used in order to create a self-assemble monolayer (SAM) on the gold surface of the thiol ends of the molecules effectively [51, 52].

In samples taken from supernatant in DI-$H_2O$ experiments, A260 / A280 ratios were not in trend with nanoparticle concentrations. DIW was then replaced with ethanol. Following the immobilization of thiol with 100% ethanol, the nanoparticles adhered

to the glass tube while separating the vancomycin that was left in solution with the magnetic separator. They were separated by half an hour sonication. Therefore, after this experiment, 9:1 ethanol and DI-$H_2O$ ratio was used for immobilization. In experiments carried out in this way, A260 / A280 values taken between 2 hours and 20 hours according to the Au-$Fe_3O_4$ concentration were within the desired ranges.

If we look at the results of the experiment, we see that the optimal amount of NPs-1 is 1.6 x $10^9$. Based on the results obtained in 2 hours, this concentration reached desired range of 1.8 of A260 / A280 ratio. The reason for decreasing values as the functionalized NP concentration increases may be due to the increase in particle aggregation colloidally. The reason why NPs-3 gives relatively low results in 2 hour experiments may be due to the low surface-to volume ratio compared to NPs-1. At the vancomycin incubation phase, images of samples of varying concentrations were in the Figure 3.8.

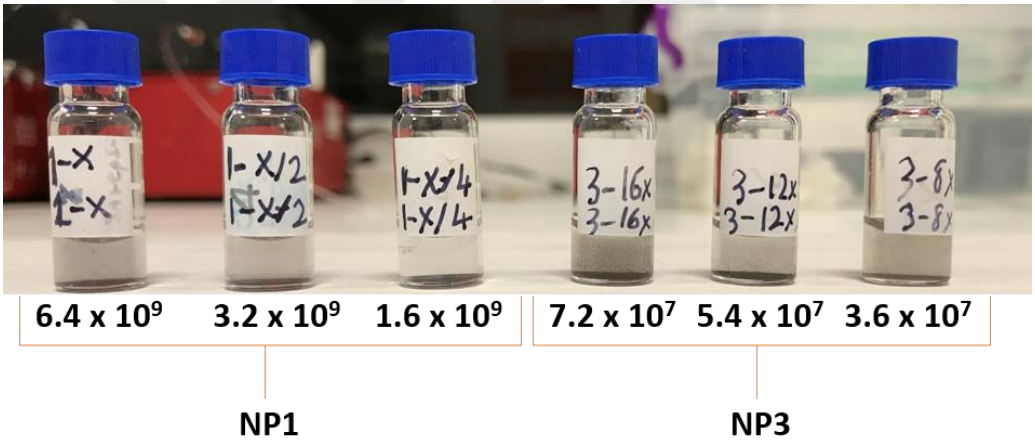


**Figure 3.8** Photography image of samples of vancomycin functionalized core-shell $Fe_3O_4$-Au nanoparticles and their approximated particle amounts.

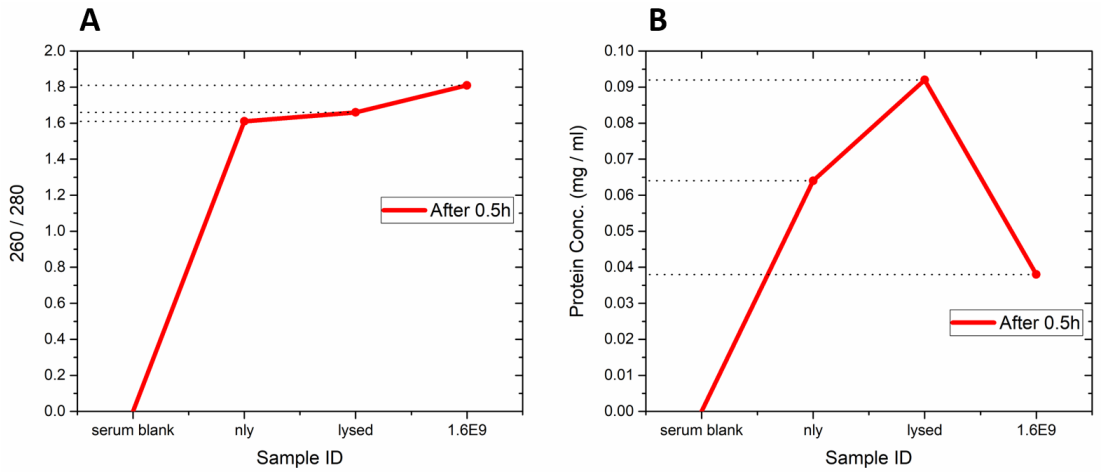


**Figure 3.9** Spectrophotometric results of approximated 1.6 x $10^9$ nanoparticles incubated in average amount of 7.5 x $10^7$ *staphylococcus aerus* after magnetic separation. **A.** 260 / 280 absorption ratio of NPs-1-Cell adsorption showing short time incubation (0.5h) efficiency. **B.** Protein concentration values dropped from 0.09 to 0.04 mg / ml (about % 44) after off-chip separation. Non-lysed sample abbreviated as 'nly'.

As a result of the experiments in Figure 3.7, NPs-1 was found suitable for on-chip experiments. The reason for this was that it could reach the rate of 1.80 in a short time. However, the lysis step was omitted in experiments in Figure 3.7. The reason for this was to try whether ethanol experiments work or not. Then, cell lysis was done with probe sonicator and lysed cells were incubated with the nanoparticle concentration with the best result (1.6 x $10^9$). Spectrophotometric measurement was taken after half an hour incubation. (Figure 3.9). The reason for taking the measurement in half an hour is that this time is considered optimum in on-chip experiments. Less time for incubation also reduces passive micromixing time.

### 3.4.2 On-chip Separation Analysis

Chip trials were done first by trying variables that were not included in the simulation. When water was first tried as a buffer, a lot of bubbles were observed in the glass-PDMS chip. Then, the PDMS-PDMS chip was produced and the experiments continued in this way. In the separation channel, a lot of flow mismatches were observed due to the outlet fitting pressure. To prevent this, pressure balancer was used

inside the chip, the intermediate microchannel has been removed and 200 µl pipette tip was used as outlet. First chip trials can be seen in Figure 3.10.

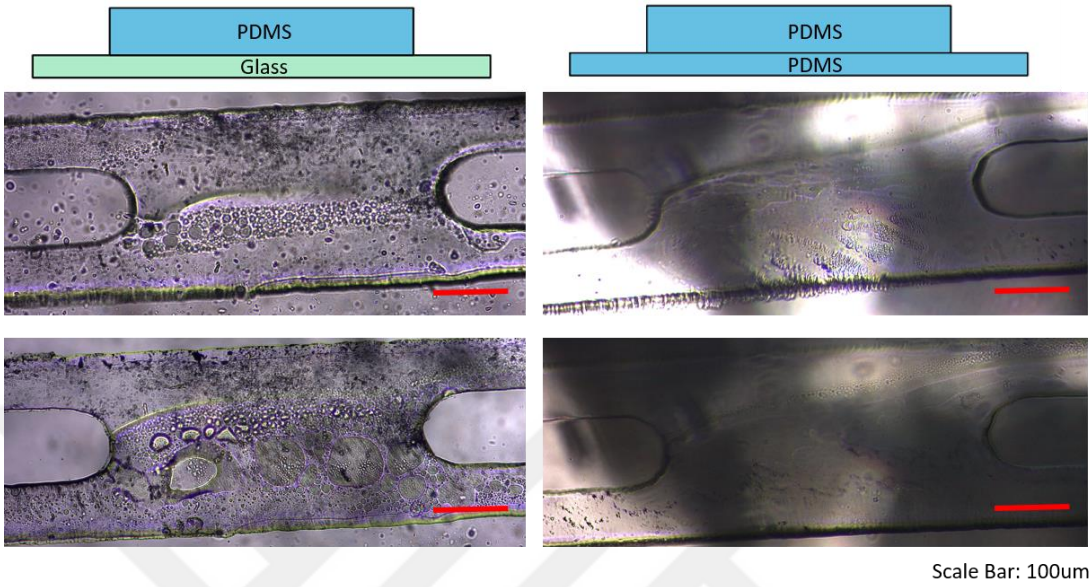


**Figure 3.10** First on-chip trials. Bubble forming can be seen on glass-PDMS mounted separation channel of the chip (left). Flow lines of the mixing clearly seen in PDMS-PDMS structure.

The final chip design consists of passive micromixing and separation sections (Figure 3.11).

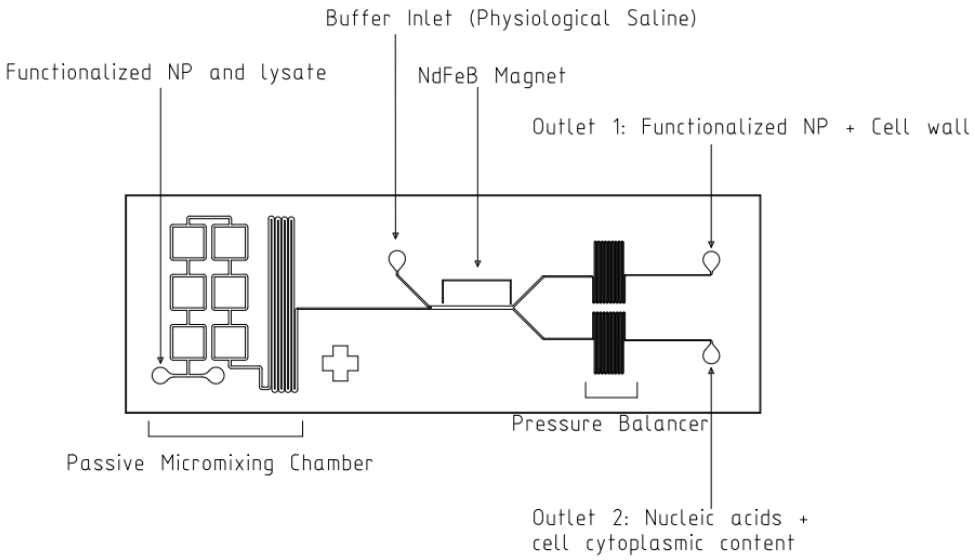


**Figure 3.11** Chip compartments.

Further experiments were done at rates of 0.75 µl / min for Inlet 1 and 0.55 µl / min for buffer inlet. Large gatherings affected by the flow and became clusters passed to Outlet 2 and trapped with the effect of magnetic effect. Due to the constant magnetic effect, black gathering places were visible in the optical microscope photograph. (Figure 3.12)

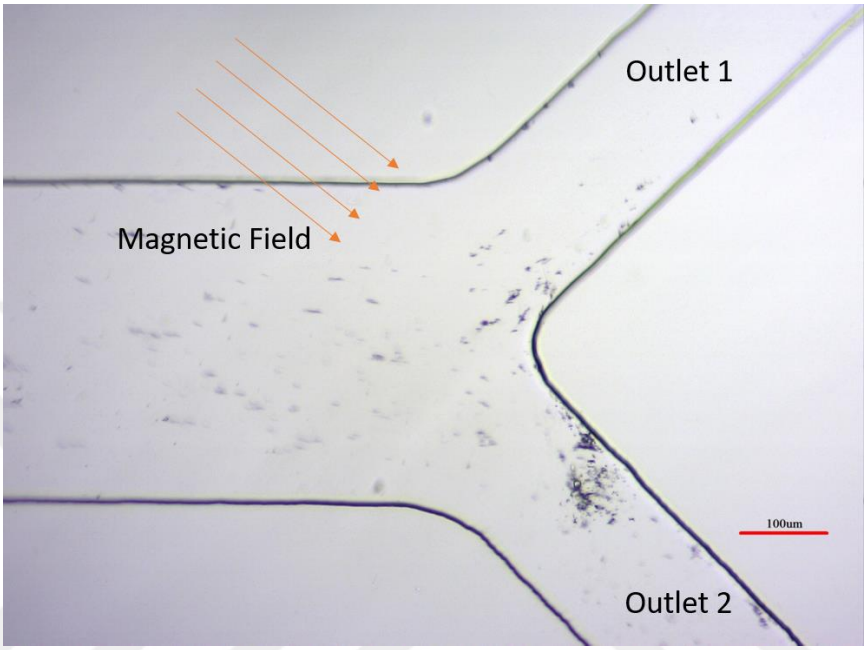


**Figure 3.12** An optical image of final part of separation channel. Large clusters can be seen along the channel.

As a result, although the simulation studies provide information about the location of the magnet and the separation channel structure, it has been understood that particle-particle interactions, hydrophilic-hydrophobic interactions can only be observed through experiments. In addition, some photoluminescence dye may be appropriate to see particle movements with magnetophoresis [53].

# CHAPTER 4

# CONCLUSION AND FUTURE DIRECTIONS

## 4.1 Conclusion

The general aim of this thesis was to use the microfluidic system to make magnetophoretic biomolecule separation for more qualified nucleic acids obtained from *S. auerus*. For this, $Fe_3O_4$ nanoparticles were synthesized successfully in different sizes and methods. The synthesized nanoparticles were between 30-300 nm in size. After nanoparticle synthesis, the nanoparticles were go through the gold deposition process and XRD and SEM characterizations were made.

Then, vancomycin molecules used as antibiotics were thiolated successfully and attached to nanoparticles. In this way, cell wall separation experiments were carried out by spectrophotometric method. In the light of the results of these methods, on-chip experiments were performed and the separation channel was examined and tried to be optimized.

For efficient separation, magnet and separation channel designs were supported by simulations and changes were made. Theoretically, magnetic flux density was found to reach the highest value of about 530 mT along the separation channel. According to the simulation, the magnet location was placed in the appropriate place for separation in the microfluidic chip

The 260/280 wavelength ratio in UV spectrograph is widely used to measure nucleic acid quality. The fact that this ratio is at the desired values indicates that the purity of the nucleic acid is less or suitable for use. For the experiments, nanoparticles of 6 different concentrations synthesized by solvo-thermal method using two separate solvents. In the experiments where the number of bacteria was constant, ($1.5 \times 10^8$ cfu / ml) the optimal nanoparticle concentration was selected for on-chip experiments ($1.6 \times 10^9$). This concentration was chosen because it allowed it to interact with and separate the bacterial cell wall in half an hour.

The importance of lab-on-chip applications has increased with the use of functionalized nanoparticles. We hope that the antibiotic functionalized nanoparticle designed in this study can serve technically and scientifically for lab-on-chip applications.

## 4.2 Future Directions

On-chip studies have not been completed yet. Although the off-chip experiments were successful, the flow velocities, passive micromixing and outlet yields in the chip will be analyzed as a result of the chip separation experiments.

The effect of passive micromixing in the chip needs to be analyzed separately. Studies continue on this section, which was designed by reviewing the literature. When particles do not mix effectively, particles under the permanent magnetic field effect tend to clump together. Thus, magnetic field dominance occurs against the flow and they cling to the separation channel. To overcome this, changes need to be made regarding micromixing efficiency, inlet speeds and buffer type.

The effect of 4-way separation channel design on simulations was successfully observed. With the magnet alignment method used in this work, magnets with different sizes and sequences can be applied to the chip.

With the completion of these studies, the chip will be turned into an integrated chip and presented to the literature for use in possible applications.

# REFERENCES


1. Hulla, J.E., Sahu, S.C. and Hayes, A.W., Nanotechnology: History and future. Human & experimental toxicology, 34(12), pp.1318-1321. 2015.

2. Merkel, T.J., Herlihy, K.P., Nunes, J., Orgel, R.M., Rolland, J.P. and DeSimone, J.M., Scalable, shape-specific, top-down fabrication methods for the synthesis of engineered colloidal particles. Langmuir, 26(16), pp.13086-13096. 2010.

3. Neužil, P., Giselbrecht, S., Länge, K., Huang, T.J. and Manz, A., Revisiting lab-on-a-chip technology for drug discovery. Nature reviews Drug discovery, 11(8), pp.620-632. 2012.

4. Thiruppathi, R., Mishra, S., Ganapathy, M., Padmanabhan, P. and Gulyás, B., Nanoparticle functionalization and its potentials for molecular imaging. Advanced Science, 4(3), p.1600279. 2017.

5. Li, J., Zou, S., Gao, J., Liang, J., Zhou, H., Liang, L. and Wu, W., Block copolymer conjugated Au-coated Fe 3 O 4 nanoparticles as vectors for enhancing colloidal stability and cellular uptake. Journal of nanobiotechnology, 15(1), pp.1-11. 2017.

6. Guzel, F.D.a.C., F., Development of an on-chip antibiotic permeability assay with single molecule detection capability. IEEE transactions on nanobioscience, 17(2), pp.155-160. 2018.

7. Cheng, I.F., Chang, H.C., Hou, D. and Chang, H.C., An integrated dielectrophoretic chip for continuous bioparticle filtering, focusing, sorting, trapping, and detecting. Biomicrofluidics, 1(2), p.021503. 2007.

8. Kartalov, E.P., Anderson, W.F. and Scherer, A., The analytical approach to polydimethylsiloxane microfluidic technology and its biological applications. Journal of nanoscience and nanotechnology, 6(8), pp.2265-2277. 2006.

9. Marghussian, V.a.M., V., Magnetic properties of nano-glass ceramics. Nano-glass ceramics. William Andrew Publishing, Oxford, pp.181-223. 2015.

10. Clemons, T.D., Kerr, R.H. and Joos, A., Multifunctional magnetic nanoparticles: Design, synthesis, and biomedical applications. In Comprehensive nanoscience and nanotechnology: Volume 3: Biological nanoscience (pp. 193-210). Elsevier BV. 2019.

11. Sinatra, F.L., Understanding the interaction between blood flow and an applied magnetic field. Graduate Theses and Dissertation. 2010.

12. Palagummi, S.a.Y., F.G., Magnetic levitation and its application for low frequency vibration energy harvesting. In Structural Health Monitoring (SHM) in Aerospace Structures (pp. 213-251). Woodhead Publishing. 2016.

13. Kotnala, R.K.a.S., J., Ferrite materials: nano to spintronics regime. In Handbook of Magnetic Materials (Vol. 23, pp. 291-379). Elsevier. 2015.

14. Glover, P.W.J., Geophysical Properties of the Near Surface Earth: Electrical Properties. Treatise on geophysics, pp.89-137. 2015.

15. Mayo-Smith, W.W., Saini, S., Slater, G., Kaufman, J.A., Sharma, P. and Hahn, P.F., MR contrast material for vascular enhancement: value of superparamagnetic iron oxide. AJR. American journal of roentgenology, 166(1), pp.73-77. 1996.

16. Guo, T., Lin, M., Huang, J., Zhou, C., Tian, W., Yu, H., Jiang, X., Ye, J., Shi, Y., Xiao, Y. and Bian, X., The recent advances of magnetic nanoparticles in medicine. Journal of Nanomaterials. 2018.

17. Mishra, D., Arora, R., Lahiri, S., Amritphale, S.S. and Chandra, N., Synthesis and characterization of iron oxide nanoparticles by solvothermal method. Protection of Metals and Physical Chemistry of Surfaces, 50(5), pp.628-631. 2014.

18. Iida, H., Nakanishi, T., Takada, H. and Osaka, T., Preparation of magnetic iron-oxide nanoparticles by successive reduction–oxidation in reverse micelles: Effects of reducing agent and atmosphere. Electrochimica acta, 52(1), pp.292-296. 2006.

19. Campos, E.A., Pinto, D.V.B.S., Oliveira, J.I.S.D., Mattos, E.D.C. and Dutra, R.D.C.L., Synthesis, characterization and applications of iron oxide nanoparticles-a short review. Journal of Aerospace Technology and Management, 7(3), pp.267-276. 2015.

20. Arias, L.S., Pessan, J.P., Vieira, A.P.M., Lima, T.M.T.D., Delbem, A.C.B. and Monteiro, D.R., Iron oxide nanoparticles for biomedical applications: a perspective on synthesis, drugs, antimicrobial activity, and toxicity. Antibiotics, 7(2), p.46. 2018.

21. Khalid, M.K., Asad, M., Henrich-Noack, P., Sokolov, M., Hintz, W., Grigartzik, L., Zhang, E., Dityatev, A., Van Wachem, B. and Sabel, B.A., Evaluation of toxicity and neural uptake in vitro and in vivo of superparamagnetic iron oxide nanoparticles. International journal of molecular sciences, 19(9), p.2613. 2018.

22. Kim, M.C., Kim, D.K., Lee, S.H., Amin, M.S., Park, I.H., Kim, C.J. and Zahn, M., Dynamic characteristics of superparamagnetic iron oxide nanoparticles in a viscous fluid under an external magnetic field. IEEE Transactions on Magnetics, 42(4), pp.979-982. 2006.

23. Jones, P.V., Salmon, G.L. and Ros, A., Continuous separation of DNA molecules by size using insulator-based dielectrophoresis. Analytical chemistry, 89(3), pp.1531-1539. 2017.

24. Yu, D., Blankert, B., Viré, J.C. and Kauffmann, J.M., Biosensors in drug discovery and drug analysis. Analytical letters, 38(11), pp.1687-1701. 2005.

25. Salafi, T., Zeming, K.K. and Zhang, Y., Advancements in microfluidics for nanoparticle separation. Lab on a Chip, 17(1), pp.11-33. 2017.

26. Salafi, T., Zhang, Y. and Zhang, Y., A review on deterministic lateral displacement for particle separation and detection. Nano-Micro Letters, 11(1), p.77. 2019.

27. Shields IV, C.W., Reyes, C.D. and López, G.P., Microfluidic cell sorting: a review of the advances in the separation of cells from debulking to rare cell isolation. Lab on a Chip, 15(5), pp.1230-1249. 2015.

28. Deshpande, S., Birnie, A. and Dekker, C., On-chip density-based purification of liposomes. Biomicrofluidics, 11(3), p.034106. 2017.

29. Springston, S.R., Myers, M.N. and Giddings, J.C., Continuous particle fractionation based on gravitational sedimentation in split-flow thin cells. Analytical Chemistry, 59(2), pp.344-350. 1987.

30. Karle, M., Miwa, J., Czilwik, G., Auwärter, V., Roth, G., Zengerle, R. and von Stetten, F., Continuous microfluidic DNA extraction using phase-transfer magnetophoresis. Lab on a Chip, 10(23), pp.3284-3290. 2010.

31. Joensson, H.N., Uhlén, M. and Svahn, H.A., Droplet size based separation by deterministic lateral displacement—separating droplets by cell-induced shrinking. Lab on a Chip, 11(7), pp.1305-1310. 2011.

32. Cima, I., Wen Yee, C., Iliescu, F.S., Min Phyo, W., Hon Lim, K., Iliescu, C. and Han Tan, M., Label-free isolation of circulating tumor cells in microfluidic devices: Current research and perspectives. Biomicrofluidics, 7(1), p.011810. 2013.

33. Munaz, A., Shiddiky, M.J. and Nguyen, N.T. , Recent advances and current challenges in magnetophoresis based micro magnetofluidics. Biomicrofluidics, 12(3), p.031501. 2018.

34. Hejazian, M.a.N., N.T., A rapid magnetofluidic micromixer using diluted ferrofluid. Micromachines, 8(2), p.37. 2017.

35. Galambos, P.C., Hopkins, M.M., Rahimian, K., Martin, J.E., Anderson, G.R., Clem, P.G., Rohwer, L.E.S., Lemp, T., Derzon, M.S. and James, C.D., Magnetophoretic bead trapping in a high-flowrate biological detection system (No. SAND2004-5466). Sandia National Laboratories. 2005.

36. Furlani, E.P., Magnetophoretic separation of blood cells at the microscale. Journal of Physics D: Applied Physics, 40(5), p.1313. 2007.

37. Wen, C.Y., Yeh, C.P., Tsai, C.H. and Fu, L.M., Rapid magnetic microfluidic mixer utilizing AC electromagnetic field. Electrophoresis, 30(24), pp.4179-4186. 2009.

38. Watarai, H.a.N., M., Capillary magnetophoresis of human blood cells and their magnetophoretic trapping in a flow system. Journal of chromatography A, 961(1), pp.3-8. 2002.

39. Harris, L.G., Foster, S.J. and Richards, R.G., An introduction to Staphylococcus aureus, and techniques for identifying and quantifying S. aureus adhesins in relation to adhesion to biomaterials: review. Eur Cell Mater, 4(3), pp.100-20. 2002.

40. Norouz Dizaji, A., Ding, D., Kutsal, T., Turk, M., Kong, D. and Piskin, E., In vivo imaging/detection of MRSA bacterial infections in mice using fluorescence labelled polymeric nanoparticles carrying vancomycin as the targeting agent. Journal of Biomaterials Science, Polymer Edition, 31(3), pp.293-309. 2020.

41. Chen, Y., Zhang, J., Wang, Z. and Zhou, Z., Solvothermal Synthesis of Size-Controlled Monodispersed Superparamagnetic Iron Oxide Nanoparticles. Applied Sciences, 9(23), p.5157. 2019.

42. Cheng, C., Xu, F. and Gu, H., Facile synthesis and morphology evolution of magnetic iron oxide nanoparticles in different polyol processes. New Journal of Chemistry, 35(5), pp.1072-1079. 2011.

43. Ghazanfari, L.a.K., M.E., Simulation and experimental results of optical and thermal modeling of gold nanoshells. Materials Science and Engineering: C, 42, pp.185-191. 2014.

44. Rikken, R.S., Nolte, R.J., Maan, J.C., van Hest, J.C., Wilson, D.A. and Christianen, P.C., Manipulation of micro-and nanostructure motion with magnetic fields. Soft Matter, 10(9), pp.1295-1308. 2014.

45. Fiorillo, F., Measurements of magnetic materials. Metrologia, 47(2), p.S114. 2010.

46. Shirzadfar, H., Nadi, M., Kourtiche, D., Yamada, S. and Hauet, T., Needle-type GMR sensor to estimate the magnetic properties of diluted ferrofluid for biomedicine application. IRBM, 36(3), pp.178-184. 2015.

47. Singh, H., Du, J., Singh, P., Mavlonov, G.T. and Yi, T.H., Development of superparamagnetic iron oxide nanoparticles via direct conjugation with ginsenosides and its in-vitro study. Journal of Photochemistry and Photobiology B: Biology, 185, pp.100-110. 2018.

48. Mahmoudi, M., Shokrgozar, M.A., Simchi, A., Imani, M., Milani, A.S., Stroeve, P., Vali, H., Häfeli, U.O. and Bonakdar, S., Multiphysics flow modeling and in vitro toxicity of iron oxide nanoparticles coated with poly (vinyl alcohol). The Journal of Physical Chemistry C, 113(6), pp.2322-2331. 2009.

49. Gu, H., Ho, P.L., Tong, E., Wang, L. and Xu, B., Presenting vancomycin on nanoparticles to enhance antimicrobial activities. Nano letters, 3(9), pp.1261-1263. 2003.

50. Tataurov, A.V., You, Y. and Owczarzy, R., Predicting ultraviolet spectrum of single stranded and double stranded deoxyribonucleic acids. Biophysical chemistry, 133(1-3), pp.66-70. 2008.

51. Altintas, Z., Surface plasmon resonance based sensor for the detection of glycopeptide antibiotics in milk using rationally designed nanoMIPs. Scientific reports, 8(1), pp.1-12. 2018.

52. Lacour, V., Moumanis, K., Hassen, W.M., Elie-Caille, C., Leblois, T. and Dubowski, J.J., Formation kinetics of mixed self-assembled monolayers of alkanethiols on GaAs (100). Langmuir, 35(13), pp.4415-4427. 2017.

53. Sahoo, Y., Goodarzi, A., Swihart, M. T., Ohulchanskyy, T. Y., Kaur, N., Furlani, E. P., & Prasad, P. N., Aqueous ferrofluid of magnetite nanoparticles: fluorescence labeling and magnetophoretic control. The Journal of Physical Chemistry B, 109(9), 3879-3885. 2005.

# CURRICULUM VITAE


**PERSONAL INFORMATION**

**Name Surname** : **Yasin ÖZTÜRK**

**Date of Birth** : **04.03.1992**

**Phone** : **+90 541 605 44 87**

**E-mail** : **yasinozturk08@gmail.com**


**EDUCATION**

**High School** : **Rize Pazar Anadolu Lisesi**

**Bachelor** : **Ankara Yıldırım Beyazıt University**

**Metallurgical and Materials Engineering**

**Master Degree** : **Ankara Yıldırım Beyazıt University**

**Material Engineering**

**WORK EXPERIENCE**

- **Ankara Yıldırım Beyazıt University** **06/2018 - 08/2020**

**Master Fellow**

- **Metallurgical and Materials Engineer** **03/2018 - 08/2018**

**Company: Özgür Döküm LTD. ŞTİ.**

**Site Engineer**

- **Materials Engineer & Designer** **06/2017 - 05/2018**

**Company: FABELLAM Lamine Cam LTD. ŞTİ.**

**Site Chief**

**RESEARCH INTEREST**

- Nanotechnology
- Nanomaterial synthesis and characterization
- Thin film technology
- Micromilling
- Lab-on-a-chip
- Biosensors
- Electrochemical sensing